

Using Spectral Estimation Techniques in Adaptive Processing Antenna Systems

W. F. GABRIEL

*Electromagnetics Branch
Radar Division*

October 9, 1985



NAVAL RESEARCH LABORATORY
Washington, D.C.

SECURITY CLASSIFICATION OF THIS PAGE

REPORT DOCUMENTATION PAGE					
1a. REPORT SECURITY CLASSIFICATION UNCLASSIFIED			1b. RESTRICTIVE MARKINGS		
2a. SECURITY CLASSIFICATION AUTHORITY		3. DISTRIBUTION / AVAILABILITY OF REPORT			
2b. DECLASSIFICATION / DOWNGRADING SCHEDULE		Approved for public release; distribution unlimited.			
4. PERFORMING ORGANIZATION REPORT NUMBER(S) NRL Report 8920			5. MONITORING ORGANIZATION REPORT NUMBER(S)		
6a. NAME OF PERFORMING ORGANIZATION Naval Research Laboratory		6b. OFFICE SYMBOL (if applicable) Code 5370	7a. NAME OF MONITORING ORGANIZATION		
6c. ADDRESS (City, State, and ZIP Code) Washington, DC 20375-5000			7b. ADDRESS (City, State, and ZIP Code)		
8a. NAME OF FUNDING / SPONSORING ORGANIZATION Naval Air Systems Command		8b. OFFICE SYMBOL (if applicable)	9. PROCUREMENT INSTRUMENT IDENTIFICATION NUMBER		
8c. ADDRESS (City, State, and ZIP Code) Washington, DC 20361			10. SOURCE OF FUNDING NUMBERS		
			PROGRAM ELEMENT NO. 61153N	PROJECT NO.	TASK NO. WR021 01000
					WORK UNIT ACCESSION NO. DN680-044
11. TITLE (Include Security Classification) Using Spectral Estimation Techniques In Adaptive Processing Antenna Systems					
12. PERSONAL AUTHOR(S) Gabriel, W. F.					
13a. TYPE OF REPORT Interim		13b. TIME COVERED FROM _____ TO _____	14. DATE OF REPORT (Year, Month, Day) 1985 October 9		15. PAGE COUNT 43
16. SUPPLEMENTARY NOTATION					
17. COSATI CODES			18. SUBJECT TERMS (Continue on reverse if necessary and identify by block number)		
FIELD	GROUP	SUB-GROUP	Adaptive arrays Spectral analysis Optimal estimation		
			Antennas Tracking Spatial filters		
			Nonlinear processing Digital processing		
19. ABSTRACT (Continue on reverse if necessary and identify by block number)					
<p>Improved spectral estimation techniques are becoming a valuable asset in adaptive processing array antenna systems. They are invaluable because of the amount of additional useful information they can provide about the interference environment, utilizing only a relatively small number of degrees-of-freedom (DOF). The "superresolution" capabilities, estimation of coherence, and relative power level determination serve to complement and refine the data from faster conventional estimation techniques.</p> <p>This report discusses two conceptual application area examples that use such techniques; partially-adaptive low-sidelobe arrays, and fully-adaptive tracking arrays. For the partially-adaptive area, the information is used for the efficient assignment of a limited number of DOF in a beamspace constrained adaptive system to obtain a stable mainbeam, retention of low sidelobes, considerably faster response, and</p> <p style="text-align: right;">(Continued)</p>					
20. DISTRIBUTION / AVAILABILITY OF ABSTRACT <input type="checkbox"/> UNCLASSIFIED/UNLIMITED <input checked="" type="checkbox"/> SAME AS RPT. <input type="checkbox"/> DTIC USERS			21. ABSTRACT SECURITY CLASSIFICATION UNCLASSIFIED		
22a. NAME OF RESPONSIBLE INDIVIDUAL William F. Gabriel			22b. TELEPHONE (Include Area Code) (202) 767-2584		22c. OFFICE SYMBOL Code 5370

DD FORM 1473, 84 MAR

83 APR edition may be used until exhausted.
All other editions are obsolete.

SECURITY CLASSIFICATION OF THIS PAGE

19. ABSTRACT (Continued)

reduction in overall cost. These benefits are demonstrated via simulation examples computed for a 16-element linear array. For the fully adaptive tracking array area, the information is used in an all-digital processing system concept to permit stable nulling of coherent interference sources in the mainbeam region, efficient assignment/control of the available DOF, and greater flexibility in time-domain adaptive filtering strategy.

CONTENTS

INTRODUCTION	1
PARTIALLY-ADAPTIVE LOW-SIDELobe ANTENNAS	1
Low-Sidelobe Eigenvector Constraint	2
Low-Sidelobe Constraints for a General Beamformer	6
Interference Sources in the Mainbeam Region	9
SOURCE ESTIMATION AND BEAM ASSIGNMENT	9
AN ADAPTIVE ARRAY TRACKING APPLICATION	16
Coherent Spatial Interference Sources	16
All-Digital Tracking System Concept	18
CONCLUSIONS	20
REFERENCES	21
APPENDIX A — Snapshot Signal Model	23
APPENDIX B — Eigenvalue/Eigenvector Decomposition	26
APPENDIX C — Tracking Beams and Adaptive Distortion	33
APPENDIX D — Forward-Backward Subaperture Averaging	37

USING SPECTRAL ESTIMATION TECHNIQUES IN ADAPTIVE PROCESSING ANTENNA SYSTEMS

INTRODUCTION

Improved spectral estimation techniques are an emerging technology which derives largely from modern spectral estimation theory of the past decade and adaptive array processing techniques [1,2,3]. Coupled with the phenomenal advances in digital processing, these techniques are becoming a valuable asset for adaptive array antenna systems. Their value lies in the considerable amount of additional useful information which they can provide about the environment while using only a relatively small number of degrees-of-freedom (DOF). For example, current spectral estimation algorithms can provide asymptotically unbiased estimates of the number of interference sources, source directions, source strengths, and any cross-correlations (coherence) between sources [4,5]. Such information can then be used to track and "catalogue" interference sources, hence assign adaptive DOF.

These newer techniques are not viewed as a "superresolution" replacement for more conventional estimation methods such as mainbeam search, analogue beamformers, or spatial discrete Fourier transforms (DFT); but rather, the new technology is considered complementary to the other methods and best used in tandem. For example, "superresolution" techniques cannot compete with the speed of a DFT. Some comparisons of the various methods may be found described in the literature [3,5,6].

The purpose of this report is to present two conceptual application areas that use spectral estimation techniques, partially-adaptive low-sidelobe antennas, and fully-adaptive tracking arrays. In a partially adaptive array only a part of the DOF, array elements or beams, is individually controlled adaptively [7,8,9]. Obviously, the fully adaptive configuration is preferred since it offers the most control over the response of the antenna system. But, when the number of elements or beams becomes moderately large (hundreds), the fully adaptive processor implementation can become prohibitive in cost, size, and weight.

This report is divided into three principal parts. The second section of this report discusses partially-adaptive, low-sidelobe antennas with the focus upon a constrained beamspace system. In the third section of the report, the source estimation and beam assignment from *superresolution* techniques are considered; and in the fourth section, an all-digital, fully-adaptive tracking array concept is discussed. Several Appendices are also used for referral of the more tedious details.

PARTIALLY-ADAPTIVE LOW-SIDELOBE ANTENNAS

The antenna system, addressed in this section, is assumed to be a moderately large aperture array of low-sidelobe design wherein the investment is already considerable and one simply could not afford to make it fully adaptive. The assumption of low-sidelobes (30 dB or better) is intended to give us good initial protection against modest interference sources and to reduce the problems from strong sources, i.e., in regard to the number of adaptive DOF required and the adaptive dynamic range of the processor. Thus, retention of the low sidelobes is considered a major goal in our adaptive system. In the discussion that follows it is shown that using improved spectral estimation techniques in such a system can result in the following benefits over a fully adaptive array system:

- a. Reduction in overall cost because relatively few adaptive DOF are implemented.
- b. Simple adaptive weight constraints permit minimal degradation of the mainbeam and sidelobe levels.
- c. Reduction in computation burden.
- d. Considerably faster adaptive response.
- e. Compatibility with a larger number of adaptive algorithms, including analogue versions.
- f. Greater flexibility in achieving a "tailored" response due to greater information available.

On the negative side, a partially-adaptive system can never be guaranteed a cancellation performance equal to that of a fully adaptive array, and will deteriorate abruptly in performance when the interference situation exceeds its adaptive DOF. These risks are an inherent part of the package and must be carefully weighed for any specific system application.

Low-Sidelobe Eigenvector Constraint

In this section we review how unconstrained adaptive arrays can experience very "noisy" sidelobe fluctuations and mainbeam perturbations when the data observation/integration time is not long enough, even though the quiescent mainbeam weights are chosen for low sidelobes. Consider the simple schematic shown in Fig. 1, and let us compute the complex adaptive element weights W_k from the well-known Sample Matrix Inverse (SMI) algorithm [9,10] as expressed in the following matrix notation,

$$\mathbf{W} = \mu \hat{\mathbf{R}}^{-1} \mathbf{S}^* \tag{1}$$

where:

- \mathbf{W} is the adaptive weights vector,
- $\hat{\mathbf{R}}$ is the sample covariance matrix,
- \mathbf{S}^* is the quiescent mainbeam weights vector, and μ is a constant.

* denotes the conjugate of a complex vector or matrix.

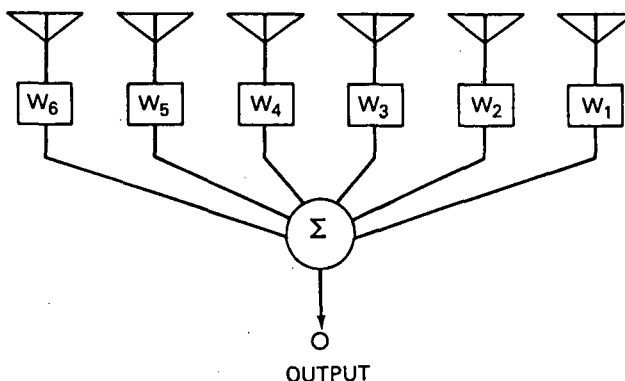


Fig. 1 – Schematic of adaptive array

Furthermore, the sample covariance matrix is computed via the simple "block" average taken over N snapshots,

$$\hat{\mathbf{R}} = \frac{1}{N} \sum_{n=1}^N \left[\mathbf{E}(n) \mathbf{E}(n)^{*t} \right], \tag{2}$$

where $\mathbf{E}(n)$ is the element signal data vector received at the n th time sampling. (See Appendix A for the description of snapshot signal model.) The data observation/integration time in (2) is the parameter N . If $\hat{\mathbf{R}}$ is estimated over a lengthy observation time, like thousands of snapshots, then the sidelobe fluctuations from \mathbf{W} updates will be relatively small. However, practical system usage often demands short observation times on the order of hundreds of snapshots or even less.

Figure 2 illustrates a typical adapted pattern behavior for independent estimates of $\hat{\mathbf{R}}$ using $N = 256$ snapshots per update for the case of three 30 dB noncoherent sources located at 14, 18 and 22°. The antenna aperture chosen for this example is a 16-element linear array with half-wavelength element spacing and a 30 dB Taylor illumination incorporated in \mathbf{S}^* . The adaptive algorithm maintains the mainbeam region and successfully nulls out the interference sources, but it also raises the sidelobe levels elsewhere. The adaptive patterns are in continual fluctuation in the sidelobe regions and may exceed the quiescent sidelobe level by a considerable margin. Also, the mainbeam suffers a significant modulation which would degrade tracking performance. These effects worsen as the value of N decreases.

To understand the reason for this undulating pattern behavior, it is helpful to analyze the optimum weights in terms of eigenvalue/eigenvector decomposition. Appendix B contains a derivation of such a decomposition for Eq. (1), and we reproduce Eq. (B-18) below:

$$\mathbf{W} = \mu' \left[\mathbf{S}^* - \sum_{i=1}^K \left(\frac{\beta_i^2 - \beta_0^2}{\beta_i^2} \right) \alpha_i \mathbf{e}_i \right] \quad (3)$$

where:

$$\alpha_i = \mathbf{e}_i^t \mathbf{S}^*$$

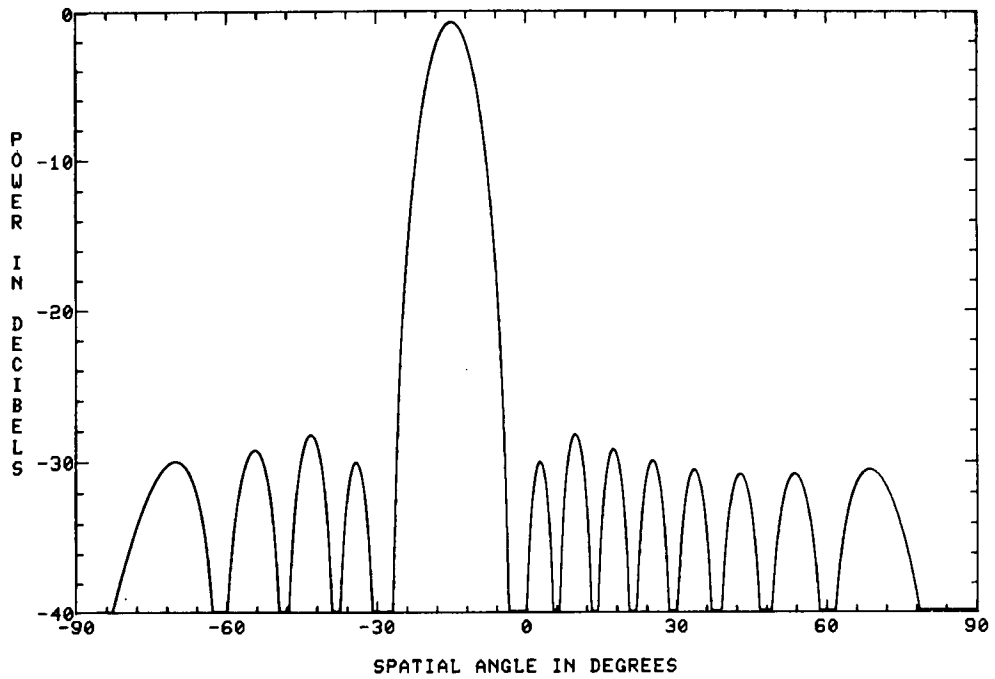
$$\mu' = \mu / \beta_0^2$$

t denotes the transpose of a vector or matrix. The β_i^2 and \mathbf{e}_i are the eigenvalues and eigenvectors, respectively, of the sample covariance matrix, and β_0^2 is equal to receiver channel noise power level. Equation (3) shows that \mathbf{W} consists of two parts: the first part is the quiescent mainbeam weight \mathbf{S}^* ; the second part, which is subtracted from \mathbf{S}^* , is the summation of weighted orthogonal eigenvectors. This is a clear expression of the fundamental principle of pattern subtraction which applies in adaptive array analysis [9,11].

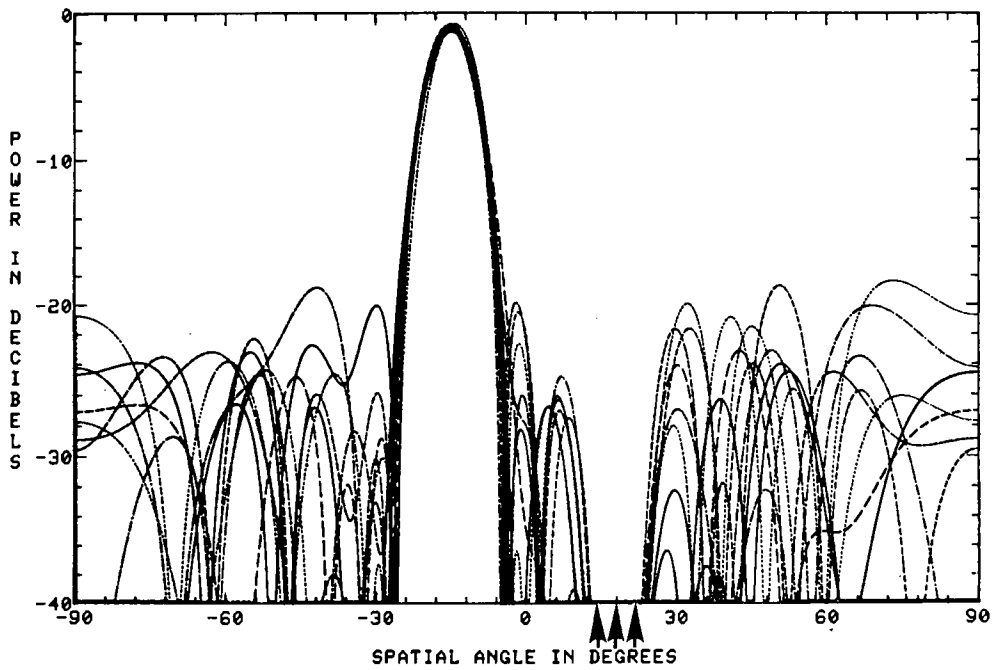
We introduce the term *principal eigenvectors* (PE) to mean those eigenvectors which correspond to unique eigenvalues generated by the spatial source distribution; and the term *noise eigenvectors* to mean those eigenvectors which correspond to the small noise eigenvalues generated by the receiver channel noise contained in the finite $\hat{\mathbf{R}}$ estimates. The PE are generally rather robust and tend to remain relatively stable from one data trial to the next, whereas the noise eigenvectors tend to fluctuate considerably because of the inherent random behavior of noise. This difference in behavior is illustrated in Fig. 3 for the three source case described above; wherein there are three PE and thirteen noise eigenvectors associated with each $\hat{\mathbf{R}}$ estimate. Figure 3(a) shows the stability of the three PE for nine trials, and Fig. 3(b) shows the random behavior of typical noise eigenvectors for the exact same trials. Thus, we would expect that the sidelobe undulations in Fig. 2(b) are associated primarily with the noise eigenvectors. This thesis is verified in Fig. 4, which illustrates the adapted patterns resulting from Eq. (3) when only the PE are subtracted.

The above adaptive array pattern behavior leads to the following observations for source distributions which do not encroach upon the mainbeam and involve a small number of the available degrees-of-freedom (DOF):

a. It is possible to retain low sidelobes in the adapted patterns, even with short observation times, by constraining our algorithm, Eq. (3), to utilize only the PE. The weight solution is unique and therefore stable.

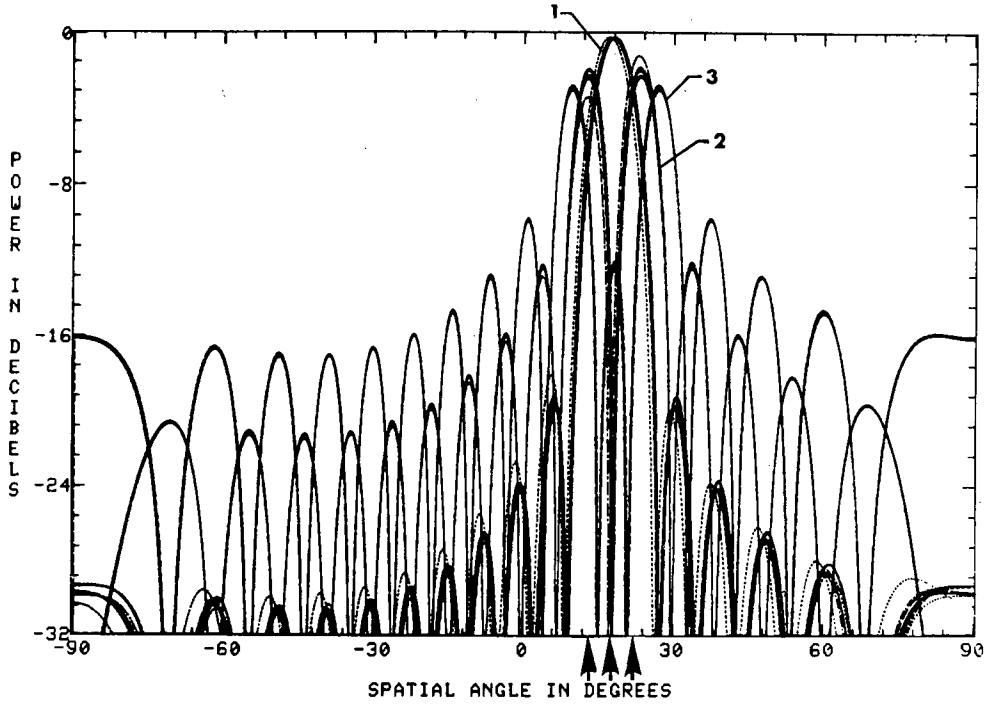


(a) Quiescent mainbeam pattern, 30 dB Taylor weighting

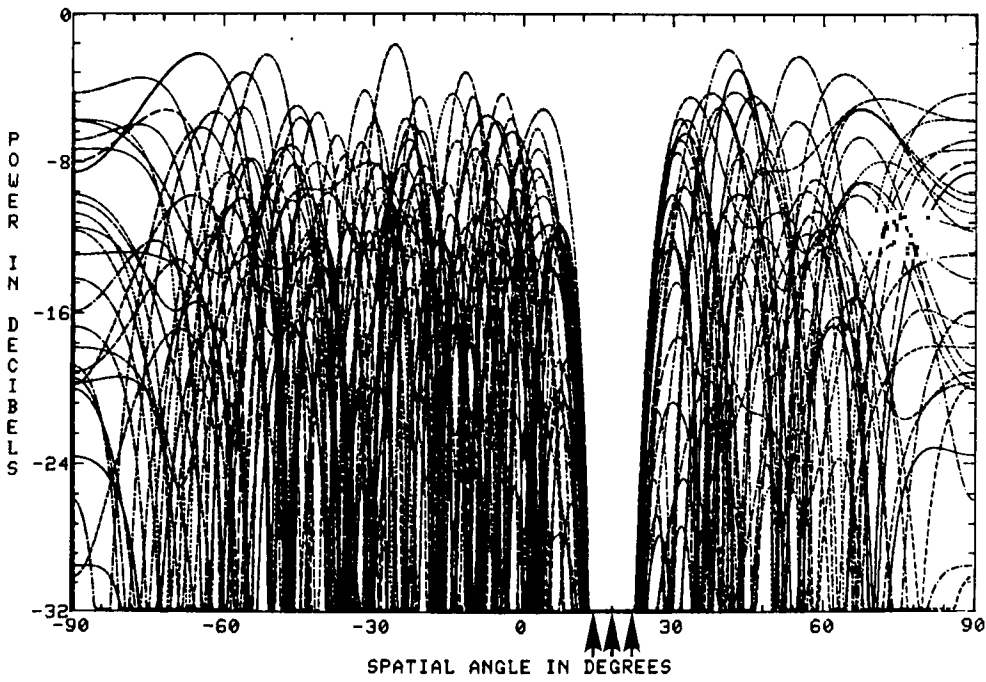


(b) Typical adapted patterns, nine update trials plotted

Fig. 2 — Fully adaptive 16-element linear array, SMI algorithm with \hat{R} estimated from 256 snapshots per update, three 30 dB non-coherent sources located at 14, 18, and 22°



(a) Principal eigenvectors (PE) Nos. 1, 2, and 3



(b) Typical noise eigenvectors Nos. 4, 10, and 16

Fig. 3 — Plots of principal eigenvectors (PE) and noise eigenvectors computed from the \hat{R} estimates associated with the three-source case of Fig. 2, nine update trials

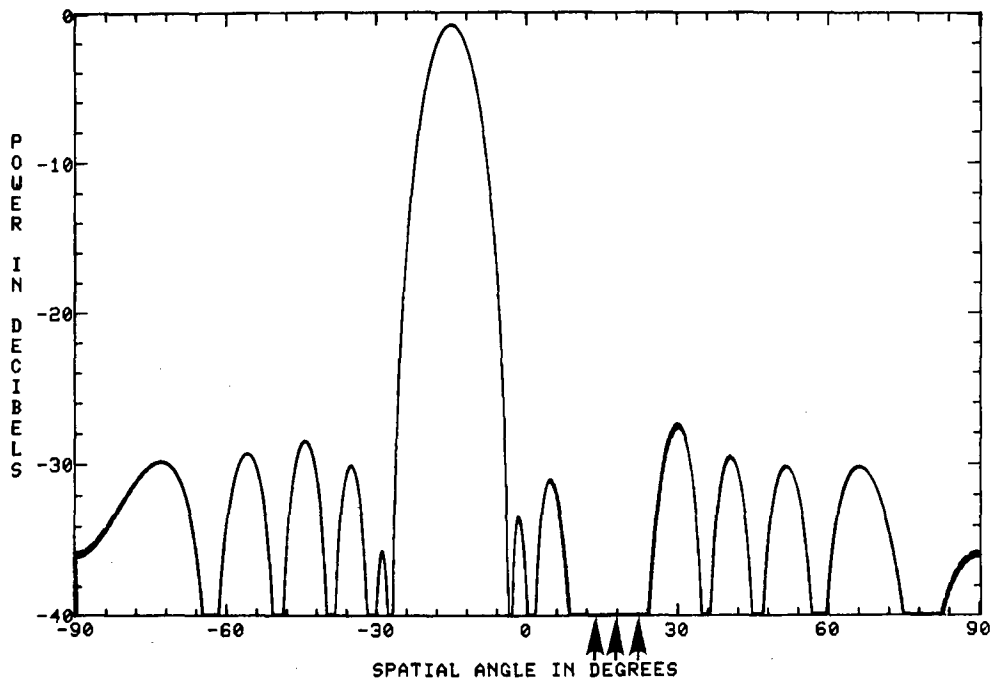


Fig. 4 — Typical adapted patterns resulting from the constraint of utilizing only the PE, three-source case of Fig. 2

b. Utilizing only the PE is tantamount to operating our adaptive system in beamspace (as opposed to element space) with a set of weighted orthogonal canceller beams.

c. The fully adaptive array automatically forms and "assigns" its PE canceller beams to cover the interference source distribution, with one beam per each DOF needed.

Therefore, we have set forth a low-sidelobe eigenvector constraint algorithm for this type of restricted interference situation.

Low-Sidelobe Constraints for a General Beamformer

Consider next a more interesting configuration which is shown by the schematic diagram in Fig. 5, where we represent an adaptive array system operating in beamspace so as to have available some pre-adaptation spatial filtering. Applebaum and Chapman [8,9,12] were the first to describe beamspace systems of this type, using a Butler matrix [13] beamformer, wherein the vector of the beamformer outputs, $\hat{\mathbf{E}}$, may be expressed as follows:

$$\hat{\mathbf{E}} = \mathbf{B}'\mathbf{E} \quad (4)$$

where \mathbf{B} is a $K \times K$ matrix containing the beamformer element weights (see Appendix C). Other descriptions of beamspace systems are also available in the literature [9,14,15,16], of which Adams et al. [15], is particularly germane to our discussion. Chapman [8] pointed out that when used in a partially adaptive configuration, such beamspace systems are susceptible to aperture element errors and cannot arbitrarily compensate the random error component of their sidelobe structure. This makes it necessary to control element errors in accordance with the quiescent mainbeam sidelobe level desired, and fits into our initial assumption of low-sidelobe design as mentioned earlier. A separate weighted

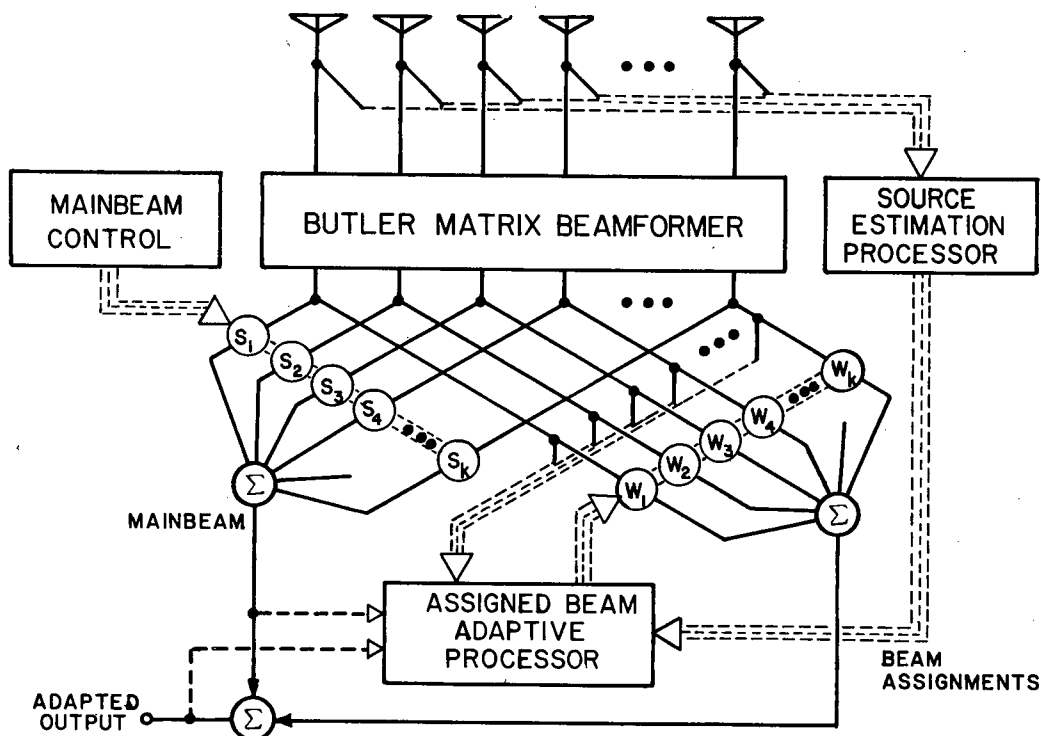


Fig. 5 — Beamspace adaptive array with a separately weighted mainbeam

mainbeam summing is indicated which may be obtained either by coupling into the beamformer outputs as shown, or by coupling off from the elements and providing suitable phase shifters for steering plus a corporate feed network. Our purpose here is to examine the sidelobe performance of such a partially-adaptive beamspace system in which element errors are kept low and beamformer beams are subjected to simple constraints.

Spatial estimation data on the interference source distribution shall determine which beamformer beams are to be adaptively controlled. Such beams are defined herein as *assigned* beams, and the idea is to assign only enough beams to accommodate the DOF required by the source distribution. Whenever the two are equal, the adaptive weight solution is unique and we avoid adding any extra "noisy" weight perturbations. The reader will recognize that we are attempting to replace the PE beams of the previous section, Low-Sidelobe Eigenvector Constraint, with assigned beams from our general beamformer. Thus, we are defining a partially-adaptive array which will utilize only a relatively small number of its available DOF. In addition to this assigned beam constraint, we seek to limit the adaptive weights of assigned beams to a maximum level, γ , which was chosen to exceed the mainbeam sidelobe level by only a few dB. This prevents an excessive rise in adaptive sidelobe level, including the condition where the number of assigned beams exceeds the DOF required.

γ represents the product of assigned beam gain and adaptive weight magnitude, so that we have the option of working with beamformer beams which are considerably decoupled/attenuated.

An equation formulation may be expressed in terms of the same pattern subtraction principle as used in Eq. (3) for K beams,

$$\mathbf{W}_0 = \mathbf{S}^* - \sum_{k=1}^K W_k \mathbf{b}_k \quad (5)$$

where:

$$\begin{aligned} |W_k| &\leq \gamma \text{ for } J \text{ assigned beams} \\ W_k &= 0 \text{ for all other beams} \end{aligned}$$

and \mathbf{b}_k is the k th Butler matrix beam element-weight vector. When $W_k = 0$, that beam port is essentially disconnected from the output summation and it is much to our advantage to reduce the DOF of the adaptive weight processor accordingly, i.e., this processor reduction relates directly to the computational burden, response time, sidelobe degradation, and overall cost mentioned earlier. For example, utilizing the SMI technique described in Eqs. (1) and (2), we would now have the advantage that our sample covariance matrix of signal inputs, $\hat{\mathbf{R}}$, involves only the J assigned beams and its dimensions reduced from $K \times K$ to $J \times J$, thereby greatly easing the computation burden involved in obtaining its inverse [9]. The equivalent "steering vector", Λ , per Applebaum [7] is also reduced to dimension J and consists of the cross-correlation between the mainbeam signal V and the J assigned beam outputs, \mathbf{Y} ,

$$\Lambda = \frac{1}{N} \sum_{n=1}^N V(n) \mathbf{Y}^*(n). \quad (6)$$

The j th assigned beam output for the n th snapshot signal sample is simply

$$Y_j(n) = \mathbf{E}'(n) \mathbf{b}_k, \quad k \text{ set by } j \quad (7)$$

where the particular value of k must be selected for the j th assigned beam. Our J dimension adaptive weight solution thus becomes,

$$\mathbf{W} = \hat{\mathbf{R}}^{-1} \Lambda. \quad (8)$$

Equation (8) gives us the J assigned beam weights required in Eq. (5). The proposed constraint $|W_k| \leq \gamma$ can be applied directly to the solution from (8), but be aware that this is a "hard" constraint and the results will not be optimal when the limit is exceeded.

A softer, more flexible constraint for our purposes is one suggested by Brennan* based upon Owsley [17], where weights are selected which simultaneously minimize both the output and the sum of the weight amplitudes squared, i.e.,

$$\text{minimize } \left\{ \overline{|V - \mathbf{W}'\mathbf{Y}|^2} + \alpha \mathbf{W}'\mathbf{W} \right\}$$

where the overbar denotes averaging over N snaps. The solution is a simple modification to Eq. (8) wherein

$$\mathbf{W} = \left[\hat{\mathbf{R}} + \alpha \mathbf{I} \right]^{-1} \Lambda \quad (9)$$

where:

$$\alpha = \left(\frac{\gamma^2}{J} \right) \text{Trace}[\hat{\mathbf{R}}].$$

We note here that Eq. (9) adds a small percentage of the average assigned beam power to the diagonal terms of $\hat{\mathbf{R}}$. We also recall that γ was selected to be close to the mainbeam sidelobe level. Although α is a small percentage of the Trace $[\hat{\mathbf{R}}]$, it is generally much larger than the receiver noise level, β_0^2 ; this domination over receiver noise by a constant will tend to severely dampen weight fluctuations due to noise. Equation (9) deviates from the optimum Weiner weights and will result in a slightly larger output residue, however, the cost is negligible compared to the remarkably stable results achieved from

*Private communication, L.E. Brennan, Adaptive Sensors, Inc.

this rather simple constraint. It essentially permits the number of assigned beams to exceed the DOF required, and yet retain low sidelobe levels.

Equations (5) through (9) were used in computing the adaptive pattern examples which follow. The reader should recognize that the J dimension adaptive weight solution may be arrived at via any of the current adaptive processing algorithms such as Howells-Applebaum [7], Gram-Schmidt [9], Sample Matrix Inverse Update [18], etc.

When applying these constraints to our three-source case of Fig. 2, we would assign beamformer beams Nos. 10, 11, and 12 to cover the sources as illustrated in Fig. 6(a). These assigned beams are then given a maximum gain level of about 5 dB above the -30 dB mainbeam sidelobes; thus, the assigned beam weights are constrained to $|W_k| \leq 0.055$. All other W_k are set to zero. Typical resultant adapted patterns are shown in Fig. 6(b), where nine trials of 160 snapshots each are plotted. The pattern stability is near-perfect for a unique solution like this, and note that the three sources have been nulled with very little perturbation of the mainbeam sidelobes except in the immediate vicinity of the sources. Since we are inverting a matrix of only 3x3 dimension in Eq. (8), for this case, it follows that the number of snapshots processed per trial could be reduced by an order of magnitude [10] and still obtain excellent results.

Figure 7 demonstrates how the adaptive weights will become *noisy* if we include even one extra DOF beyond the unique solution. Beamformer beam No. 16 was deliberately added for the same case as in Fig. 6, and we may note the consequent sidelobe fluctuations. However, if we use the "soft" constraint of Eq. (9) in solving for the weights, stable performance is again restored despite the extra DOF. It may be of interest to the reader that for this particular example:

$$\begin{aligned} J &= 4 \\ \gamma &= 0.045 \text{ (-27 dB)} \\ \text{Trace} [\hat{\mathbf{R}}] / J &\approx 10,350 \beta_0^2 \\ \alpha &= 21\beta_0^2. \end{aligned}$$

Although not shown here, another example of interest is the case of using a two-beam cluster (Nos. 11 and 12) to cancel a single 40 dB broadband source located at 22°. It was found that the source could be adequately cancelled at bandwidths up to 15%.

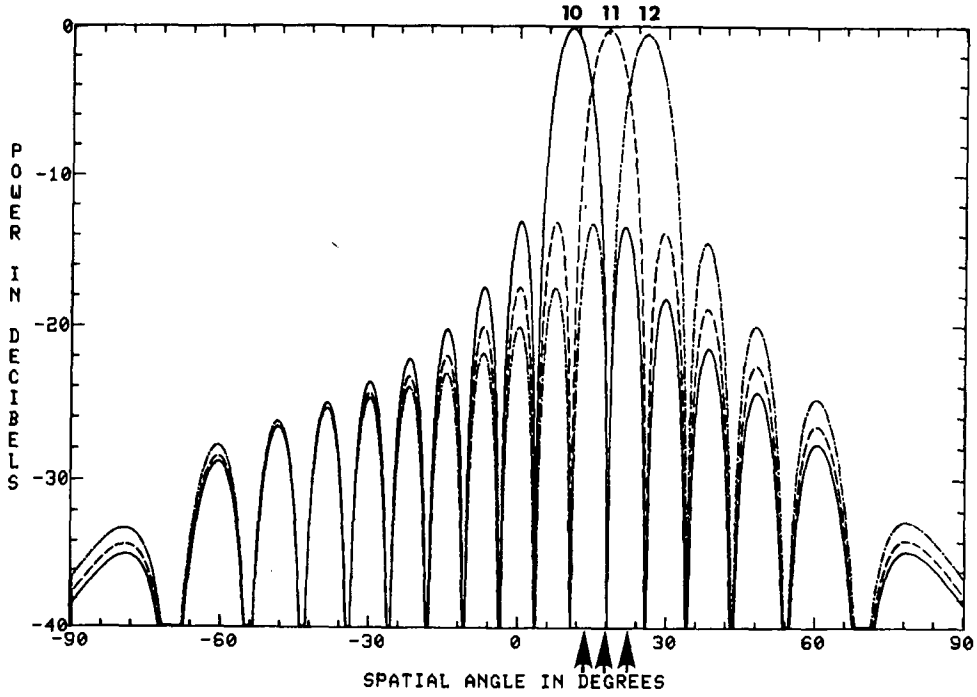
Many other combinations of source distributions and assigned beams were tested to further verify the technique, and the partially-adaptive performance was satisfactory *provided that the assigned beams were sufficient to cover the DOF demanded by the source distribution.*

Interference Sources in the Mainbeam Region

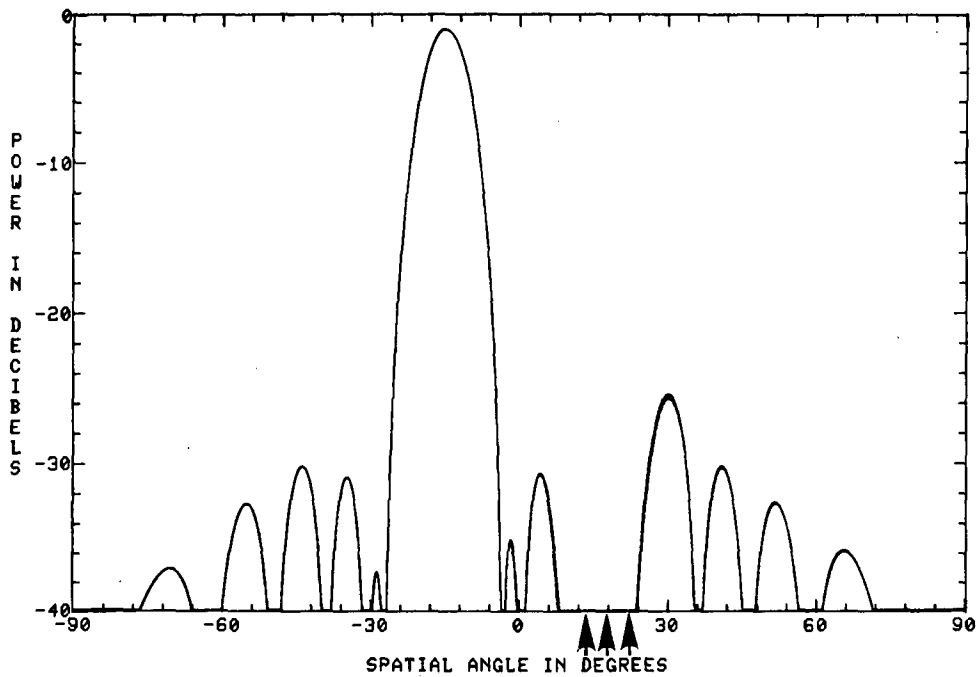
Extension of the foregoing partially-adaptive array technique for mainbeam interference is straightforward, provided we relax the constraint upon the value of γ in Eq. (5). Obviously, the low-sidelobe stratagem becomes secondary to the greater menace of an interference source coming in through our high-gain mainbeam. Low sidelobes could still be retained, if necessary, by implementing a beamformer which is capable of producing a family of low-sidelobe assigned beams [15].

SOURCE ESTIMATION AND BEAM ASSIGNMENT

Modern spectral estimation techniques are a welcome addition to the conventional methods for tracking and cataloging interference sources. They do not interfere with any functions of the mainbeam, and are capable of providing superior source resolution from fewer elements. The latter advantage is obtained in part because we assumed low sidelobes for the mainbeam, i.e., the only sources that require estimation are those few which are of sufficiently high SNR to get through the mainbeam sidelobes. Resolution performance is always directly related to SNR, [2,5,6].

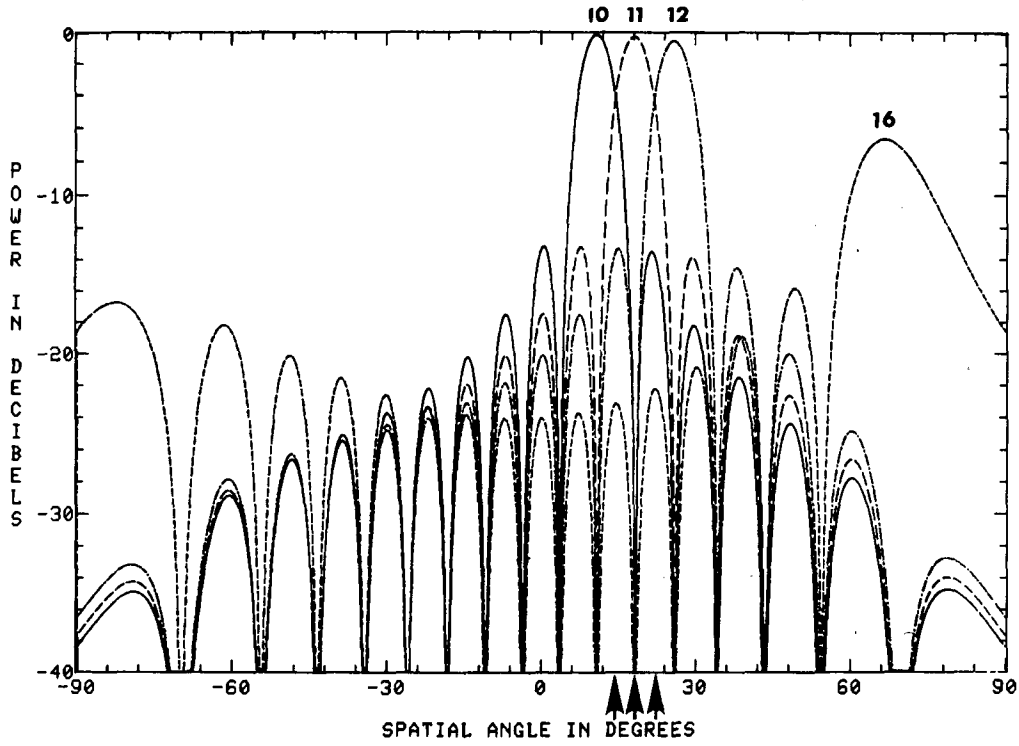


(a) Beamformer beams Nos. 10, 11, and 12

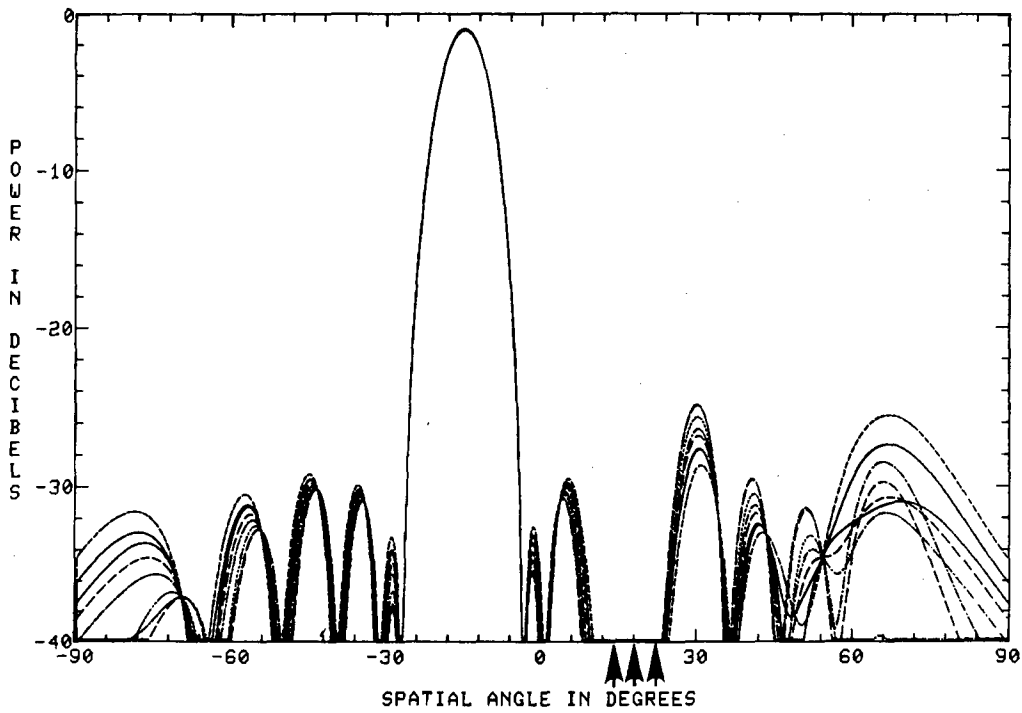


(b) Typical adapted patterns, nine trials of 160 snapshots

Fig. 6 — Partially adaptive linear array of 16 elements, using three assigned beams for the three source case of Fig. 2



(a) Beamformer beams Nos. 10, 11, 12, and 16



(b) Typical adapted patterns, nine trials of 160 snapshots

Fig. 7 — Partially adaptive linear array of 16 elements, using four assigned beams for the three-source case of Fig. 2

The principle for achieving source estimation from a small fraction of the aperture DOF has been demonstrated via many techniques, both conventional and optimal [1,3,19]. It is not within the scope of this report to attempt a comprehensive comparison of such techniques, but the point is important to our concept so that an example of a half-aperture linear array estimator is given in this section. The type of application envisioned is illustrated in Fig. 8, where we represent a $K \times K$ element aperture system in which the adaptive beam DOF are to be assigned on the basis of estimates derived from two orthogonal linear arrays of $K/2$ elements each. An extension of the 2D (two-dimension) beamspace adaptive array system of Fig. 5 to the 3D system suggested by Fig. 8 permits several beamformer options, including:

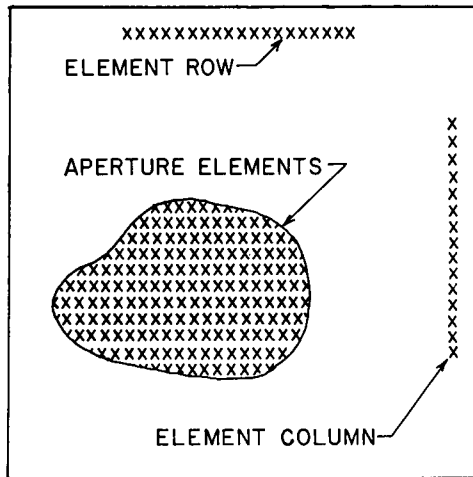


Fig. 8 - $(K \times K)$ element aperture within which row/column linear arrays couple into source estimation processors

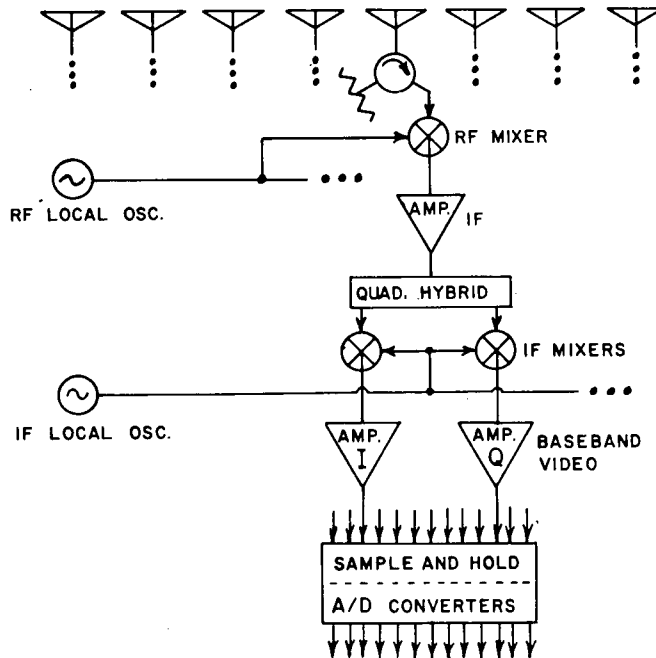


Fig. 9 - Typical RF receiver techniques associated with A/D complex data sampling

- a. Two orthogonal 2D beamformers of which one is coupled into a row and the other coupled into a column of elements.
- b. A complete 3D beamformer [20] coupled into the aperture elements, perhaps on a thinned basis.

The separate mainbeam must be summed from all K^2 elements to attain the desired low sidelobes.

Although they involve relatively few elements from the aperture, the linear array estimators represent a significant increase in system expense, because they are all-digital processing subsystems. Typical RF receiver components required prior to the signal analogue-to-digital (A/D) converters are shown in Fig. 9. The processing of the digital signals to estimate the sources may be carried out in accordance with a number of spectral estimation algorithms available in the literature [1-6]. Appendix B discusses several algorithms that were used in the simulations conducted for this report. For example, Fig. 10 illustrates a comparison plot of our mainbeam search scan vs half-aperture eigenanalysis processing results for the 16-element linear array case of Fig. 2.

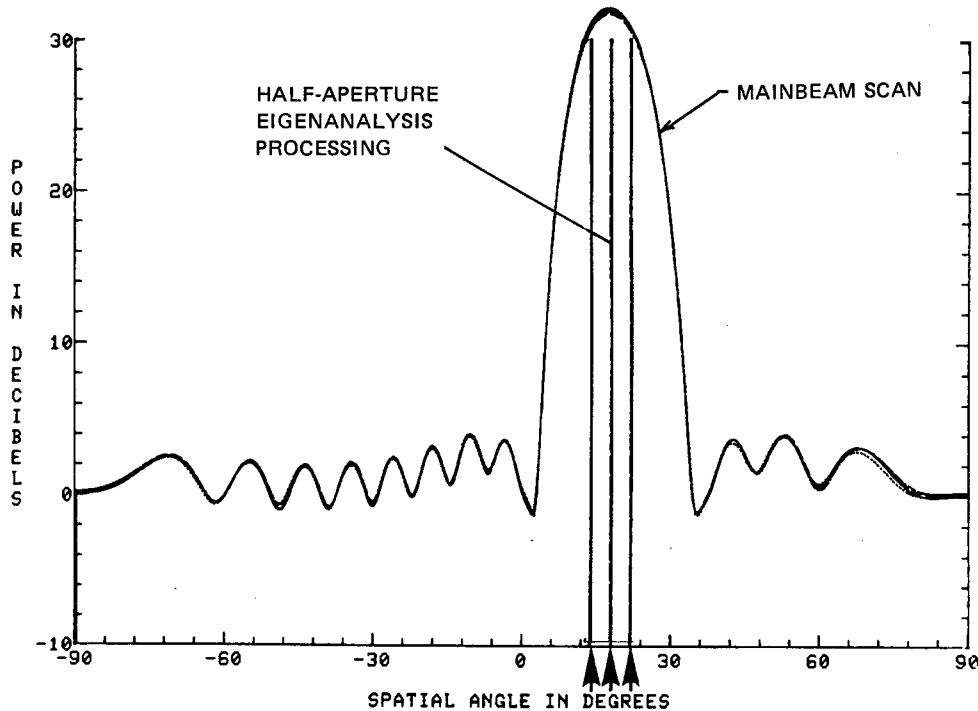


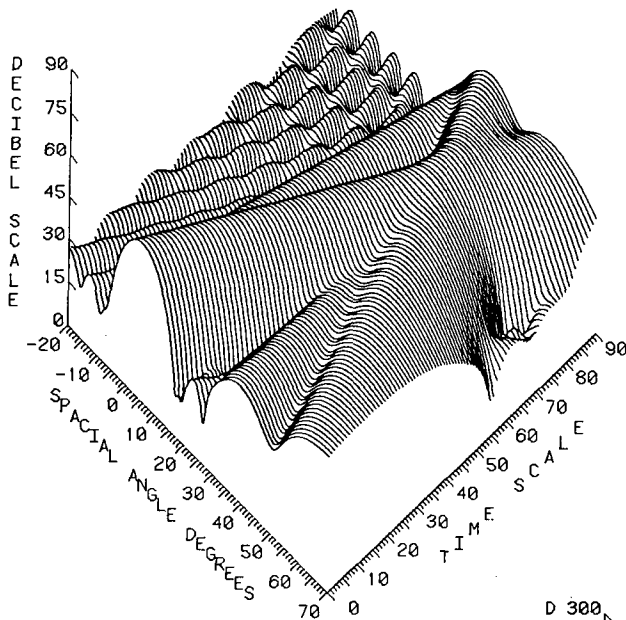
Fig. 10 — Comparison of mainbeam scan vs half-aperture eigenanalysis source estimation for three source case of Fig. 2

Once the source estimation information is available, we can proceed by assigning beamformer beams via a computer logic program. For the simulations reported in this report, a Fortran IV computer code named "BEAMASSIGN" was developed which accepts source information updates, compares the new data against a source directory kept in memory, computes track updates for sources already in memory, determines priority ranking, and assigns beams to cover the sources of highest priority. An important point to note is that beam assignment does not require great accuracy, i.e., a half-beamwidth is usually close enough. Also, clusters of two or three adjacent beams may be assigned for doubtful cases.

A demonstration of beam assignment was conducted with a moving source simulation involving the 16-element linear array of Fig. 2. Four sources of unequal strength were set up in the farfield, traveling in criss-crossing patterns. Two of the sources are of 30 dB strength with start angles of 3.0 and 39.0°, and two are of 43 dB strength with start-angles of 5.0 and 70.0°. The estimation of the scanned mainbeam for this example is shown in Fig. 11(a). Each time-unit plot cut is computed from $\hat{\mathbf{R}}$ averaged over 160 snapshots,

$$P_0 = \mathbf{S}'\hat{\mathbf{R}}\mathbf{S}^* \quad (10)$$

where \mathbf{S}^* is the mainbeam steering vector used to generate the display plot. As expected, this simple Fourier output is dominated by the two stronger sources. In contrast, Fig. 11(b) shows the source estimation derived from eigenanalysis processing using only half of the aperture (8 elements). Note that the "superresolution" characteristics of this type of optimal estimation produces excellent source tracking, even in the vicinity of cross-over of three of the sources.



(a) Conventional mainbeam scanning, 16 elements, 30 dB Taylor illumination

(b) Half aperture eigenanalysis source estimation

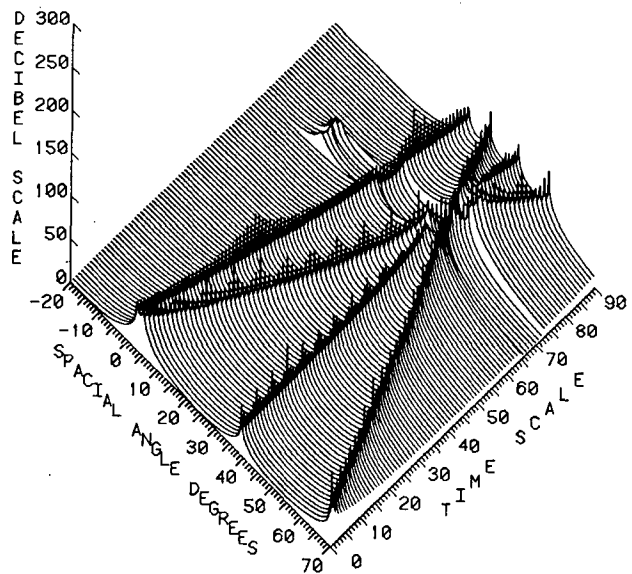
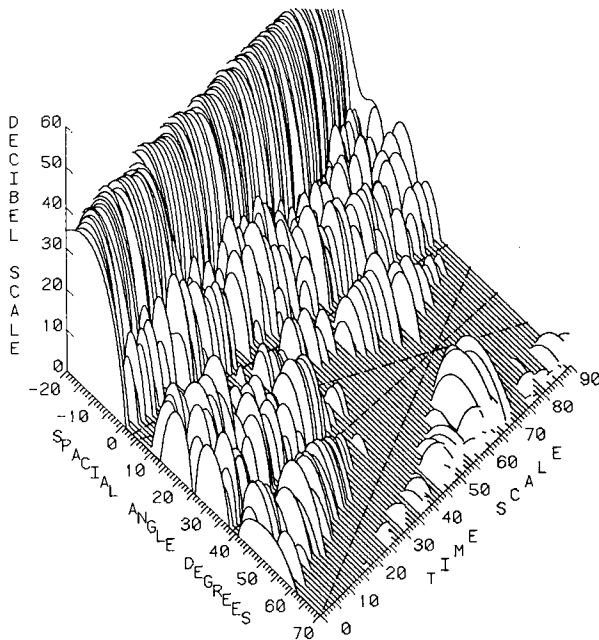
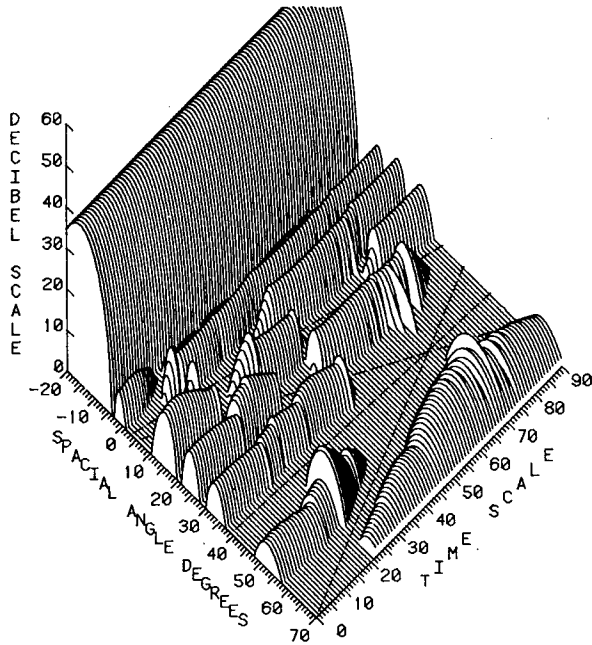


Fig. 11 — Estimation of four moving sources via mainbeam scan and half aperture eigenanalysis algorithm

The results from the use of the source information data contained in Fig. 11(b) to continuously update beam assignments are illustrated in the adapted pattern cuts shown in Fig. 12(a). Note that the mainbeam remains steady, and the sidelobes seldom exceed their quiescent 30 dB peak level, despite the drastic shifting of the nulls as the moving sources criss-cross in the sidelobe region. In contrast, Fig. 12(b) illustrates the adapted pattern cuts obtained when we utilize the SMI algorithm weights with the array fully adaptive. Although the source cancellation is excellent, the mainbeam suffers significant modulation and the peak sidelobe levels rise considerably.

(a) Partially adaptive, constrained, assigned beams, 32 snapshots processed per plot cut



(b) Fully adaptive array, no constraints, 300 snapshots processed per plot cut

Fig. 12 — Adaptive patterns for 16 element linear array, SMI algorithm, four moving sources case of Fig. 11

AN ADAPTIVE ARRAY TRACKING APPLICATION

A second area where spectral estimation techniques can provide valuable assistance is that of adaptive array tracking systems. Here we are dealing with the problem of attempting to track targets under the condition of having interference sources present in the mainbeam region. Some early proposed solutions in this area evolved from the growing adaptive array technology of the 1970's. For example, a paper by White [21] discusses the radar problem of tracking targets in the low-angle regime, where conventional tracking radars encounter much difficulty because of the presence of a strong surface-reflected ray.

The first extension of fully adaptive arrays to angle estimation in external noise fields is the contribution of Davis et al. [22], who developed an algorithm based on the outputs of adaptively distorted sum and difference beams. The adaptive beams filter (null) the external noise sources, and distortion correction is then applied in the resultant monopulse output angle estimate. Their work is particularly appropriate as a starting point for this section, where we discuss the advantages of using spectral estimation techniques in an all-digital, fully adaptive, array tracking system. Reference [15] is also pertinent.

Coherent Spatial Interference Sources

The existence of significant coherence between spatial sources as, for example, in multipath situations involving a specular reflection, continues to represent a serious problem area even for a fully adaptive tracking array.

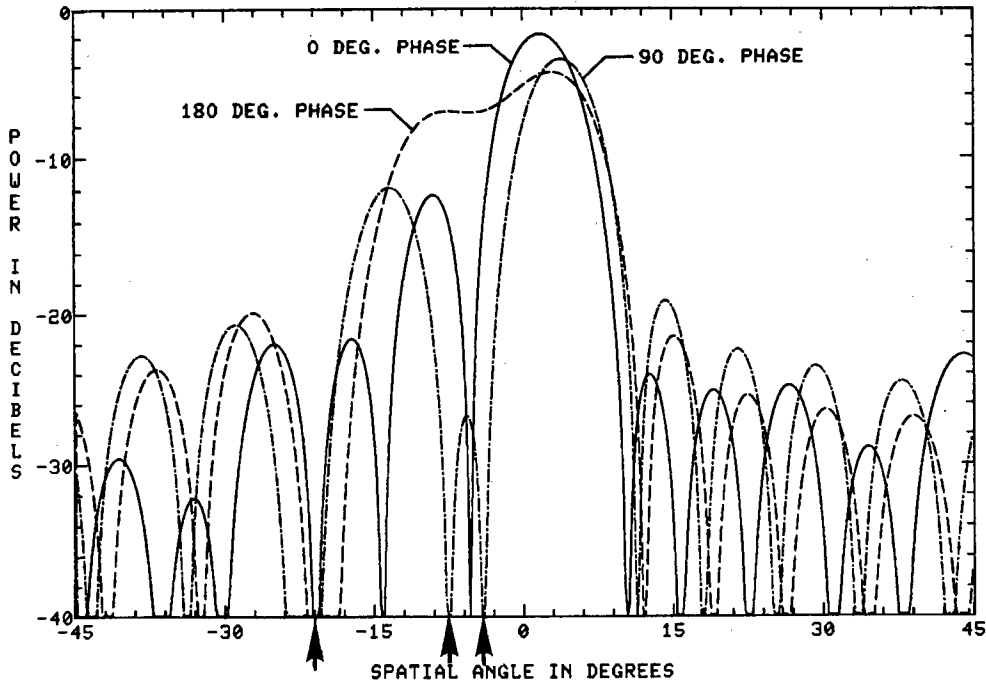
Reasons include:

- a. Coherent signals in space are not stationary [2,5,23].
- b. Adaptive systems may perform cancellation via weight phasing rather than null steering [5,23,24,25,26].
- c. Adaptive tracking beam distortion is highly sensitive to coherent signal phasing.
- d. Signal fading under anti-phase conditions.

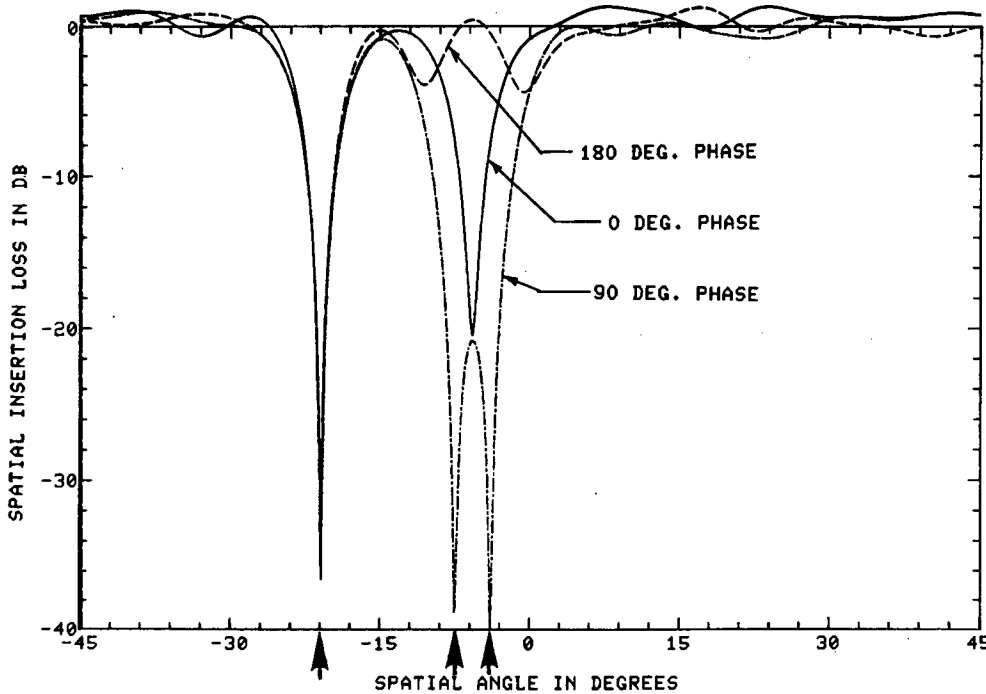
To demonstrate these reasons, adaptive characteristics were computed for a 16-element linear array for an interference case in which there are two 13 dB coherent sources in the mainbeam region. There is also a third source, non-coherent, in the nearby sidelobe region that acts as a stable null comparison point.

In Fig. 13(a), we illustrate the severe changes in our mainbeam caused by variation of the phase shift between the two coherent sources. The quiescent mainbeam has the same Taylor weighting as that in Fig. 2(a). Figure 13(b) illustrates the spatial insertion loss associated with the three adaptive weightings involved. Note that for source phasing of 0° and 180° , the adaptive weights do not achieve cancellation by steering nulls onto the coherent sources, but rather by the weight phasing itself. The array output was driven down to receiver noise level in all three cases. The plots for 90° phase are very similar to what one would obtain if all three sources were non-coherent, i.e., cancellation is achieved by adaptive null steering, in this instance.

Such severe sensitivity to coherent source phasing in the mainbeam region produces different distortions in tracking estimates from adaptive Σ (sum) and Δ (difference) patterns, as shown in Fig. 14. Appendix C contains the equation development for this type of plot; however, the main point here is to show the considerable changes in track angle estimates due to phase variation. Once again, if all three sources were non-coherent, the distortion plot would be stable and very similar to the one shown for the 90° phase.



(a) Typical adaptive patterns for three coherent phases



(b) Insertion loss associated with adaptive weighting

Fig. 13 — Mainbeam interference adaptive characteristics for 16 element linear array, SMI algorithm, 256 snapshots, three interference sources: one 10 dB non-coherent at -21° , and two 13 dB coherent at -7.6° and -4.0°

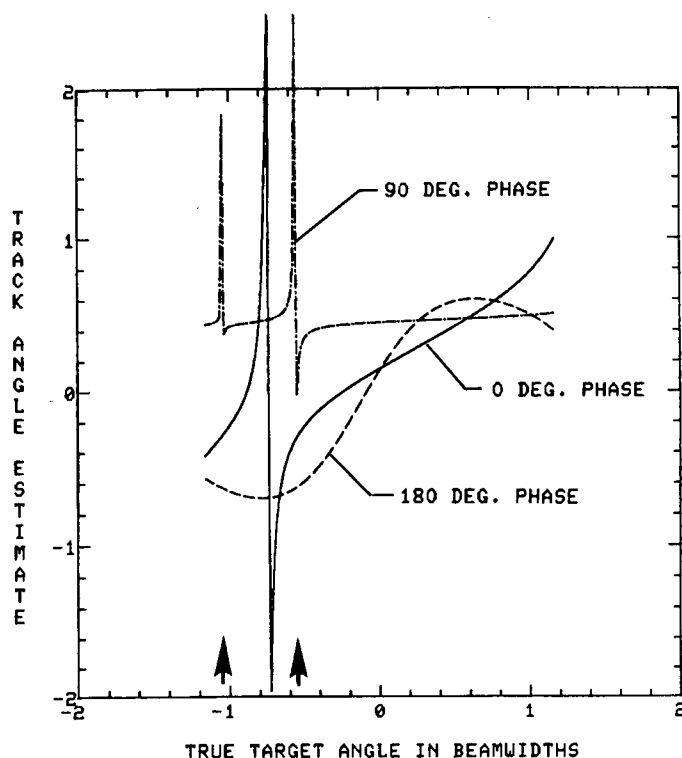


Fig. 14 — Track estimate distortion resulting from adaptive Σ and Δ tracking beams for coherent interference in the mainbeam region, same case as Fig. 13

All-Digital Tracking System Concept

The separate estimation of interference source data (total number, power levels, location angles, coherence) and its utilization for improving the output SNR of desired signal detections is a mode of system operation that has been addressed in the literature a number of times for various applications [5,6,15,16]. In this section, we briefly review such a system wherein the estimated data is used to drive a fully adaptive tracking processor [27]. The concept is illustrated in Fig. 15. Starting on the left-hand side, the system continuously computes/updates a sample covariance matrix $\hat{\mathbf{R}}$. Of particular significance is that $\hat{\mathbf{R}}$ may be dimensioned either equal to or less than the total number of array elements, i.e., the model order of the estimate is selectable per subaperture averaging option choice. Off-line processing on $\hat{\mathbf{R}}$ is then conducted at periodic intervals to estimate the locations and relative power levels of interference sources via the most appropriate spectral estimation algorithms. The central processor unit (CPU) then applies these data to the computation of optimized adaptive spatial filter weights for the right-hand side of Fig. 15. Separation of source estimation from adaptive filter weight computation can be done accurately only in an all-digital processing system, but it permits the following benefits:

- a. Estimation of coherent interference source locations for deliberate adaptive null filter placement.
- b. Remembering slow-changing or time-gated sources, and *colored-noise* distributions.
- c. Anticipating sources from apriori data inputs.

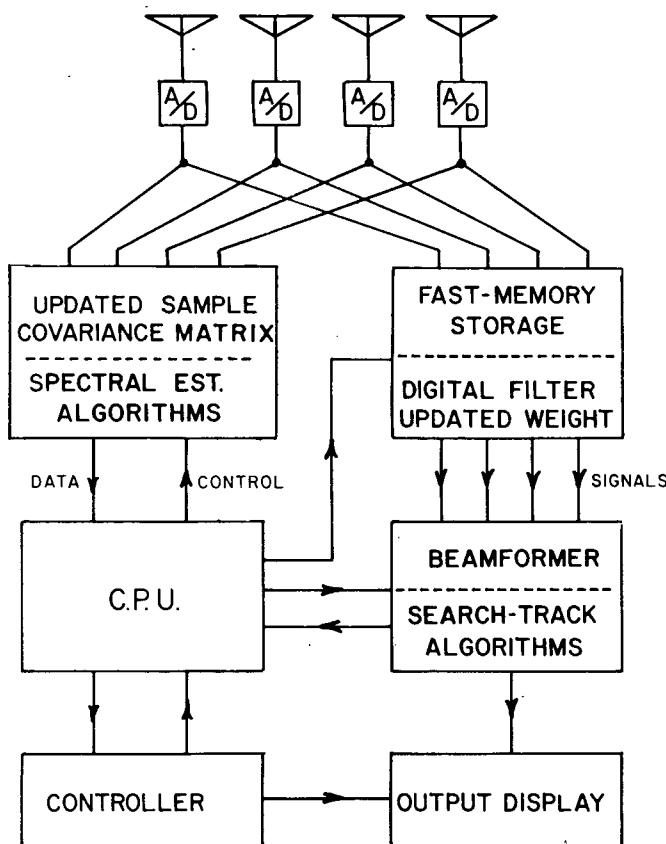


Fig. 15 — All-digital adaptive array tracking system concept

- d. Flexibility in time-domain control of the filtering to counter interference time strategies.
- e. Tracking/cataloging/ranking sources.
- f. Efficient assignment of available DOF.
- g. Compatible with fast-response adaptive algorithms, i.e., parallel algorithm processing.

The right-hand side of Fig. 15 indicates a fast-memory storage capability that is intended to permit selected time delays of the snapshots for feeding into the filter weights. The idea is to synchronize selected snapshots with their filter weight updates, if possible.

Finally, the filtered signal output residue is fed into a beamformer which is weighted to produce the desired search and monopulse track beams for target detection and tracking. The algorithms of Davis et al., [22], may be applied for estimating the target signal angle of arrival, based upon the outputs of adaptively distorted sum and difference beams. Appendix C discusses the equivalence of such beams to the concept shown in Fig. 15.

As an example, let us apply this concept to the coherent source case used in Figs. 13 and 14 wherein we would use a 16-element linear array feeding into our all-digital processor. An appropriate estimation algorithm is that of forward-backward subaperture spatial smoothing [5,28,29] combined with eigenanalysis. Appendix D describes the rudiments of this algorithm, and the results are plotted in Fig. 16 in comparison with a scanned mainbeam output. From this source estimation data, we can

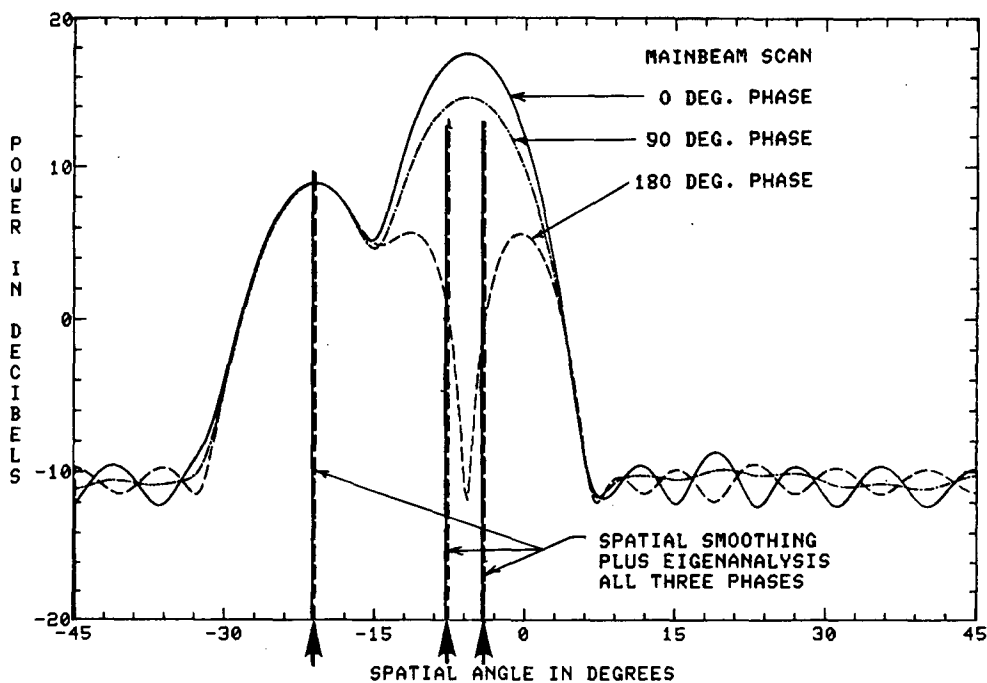


Fig. 16 — Comparison of mainbeam scan vs spatial smoothing processing for coherent source case of Fig. 13, PEGS eigenanalysis, 256 snapshots per trial

construct an equivalent covariance matrix dimensioned for the full aperture per the procedure given in Appendix A, and we can compute its inverse for obtaining the adaptive filtering. If we define the constructed covariance matrix as \mathbf{M} , then its inverse may be viewed as a matrix set of adaptive *beamformer* filter weights to give us the filtered output n th snapshot vector $\mathbf{E}_f(n)$,

$$\mathbf{E}_f(n) = \mathbf{E}'(n) \mathbf{M}^{-1} \quad (11)$$

Conventional beam weighting \mathbf{S}^* can then be applied to the filtered output residue to obtain the final output for the n th snapshot,

$$Y_0(n) = \mathbf{E}_f(n) \mathbf{S}^* = \mathbf{E}'(n) \mathbf{M}^{-1} \mathbf{S}^* \quad (12)$$

or

$$Y_0(n) = \mathbf{E}'(n) \mathbf{W}_0$$

where \mathbf{W}_0 is the familiar optimum Wiener filter weight.

Note that the constructed covariance matrix, \mathbf{M} , permits options such as adding synthetic sources or changing power levels. Furthermore, since it is always Toeplitz, solutions may be simplified somewhat.

For the current example, the computed adaptive characteristics would be very similar to those plotted in Figs. 13 and 14 for the 90° phase angle. Other examples along with a more detailed discussion of the processing may be found in [27].

CONCLUSIONS

Two conceptual application areas have been presented for using spectral estimation techniques; partially-adaptive low-sidelobe arrays, and fully-adaptive tracking arrays. In both cases, improved spectral estimation techniques are used separately to acquire information about the interference environ-

ment which is beyond that ordinarily available in a conventional adaptive array. Examples discussed included *superresolution* effects, relative power level determination, estimation of coherent sources, and the tracking/cataloging/ranking of sources. For the partially-adaptive area, the information was used for efficient assignment of a limited number of DOF in a beamspace constrained adaptive system to obtain the following benefits (as compared to a fully adaptive array): retention of low sidelobes plus a stable mainbeam; considerably faster adaptive response; reduction in overall cost; and greater flexibility. On the negative side, we incur the risk of possible inferior cancellation performance if the interference source situation is not adequately covered by the assigned DOF.

For the fully adaptive tracking array area, the information is used in an all-digital processing system to obtain the benefits of stable nulling of coherent interference sources in the mainbeam region, efficient assignment of the available DOF, and a far greater flexibility in the time-domain control of adaptive filtering strategy.

REFERENCES

1. D.G. Childers, ed., *Modern Spectrum Analysis*, IEEE Press, New York, N.Y. 1978.
2. W.F. Gabriel, "Spectral Analysis and Adaptive Array Superresolution Techniques," Proc. IEEE **68**, Jun 1980, pp. 654-666.
3. Special Issue on Spectral Estimation, Proc. IEEE **70**, Sep 1982.
4. R. Schmidt, "Multiple Emitter Location and Signal Parameter Estimation," Proc. of the RADC Spectrum Estimation Workshop, RADC-TR-79-63, Rome Air Development Center, Rome, NY, Oct 1979, p. 243.
5. J.E. Evans, J.R. Johnson, and D.F. Sun, "Application of Advanced Signal Processing Techniques to Angle of Arrival Estimation in ATC Navigation and Surveillance Systems," MIT Lincoln Laboratory Tech. Report 582, (FAA-RD-82-42), Jun 1982.
6. A.J. Barabell et al., "Performance Comparison of Superresolution Array Processing Algorithms," MIT Lincoln Laboratory Report TST-72, May 1984.
7. S.P. Applebaum, "Adaptive Arrays," IEEE Trans. Antennas Propagat., AP-24, Sep 1976, pp. 585-598.
8. D.J. Chapman, "Partial Adaptivity for the Large Array," IEEE Trans. Antenna Propag., AP-24, Sep 1976, pp. 685-696.
9. R.A. Mozingo and T.W. Miller, *Introduction to Adaptive Arrays*, (John Wiley and Sons, New York, 1980).
10. I.S. Reed, J.D. Mallett, and L.E. Brennan, "Rapid Convergence Rate in Adaptive Arrays," IEEE Trans. Aerosp. Electron, Syst., AES-10, Nov 1974, pp. 853-863.
11. W.F. Gabriel, "Adaptive Arrays — An Introduction," Proc. IEEE, **64**, Feb 1976, pp. 239-272.
12. S.P. Applebaum and D.J. Chapman, "Adaptive Arrays with Main Beam Constraints," IEEE Trans. Antennas Propagat. AP-24, Sep 1976, pp. 650-662.
13. J. Butler, "Multiple Beam Antennas," Sanders Assoc. Internal Memo RF 3849, Jan 1960.

14. J.T. Mayhan, "Adaptive Nulling with Multiple-Beam Antennas," IEEE Trans. Antennas Propag., AP-26, Mar 1978, pp. 267-273.
15. R.N. Adams, L.L. Horowitz, and K.D. Senne, "Adaptive Main-Beam Nulling for Narrow-Beam Antenna Arrays," IEEE Trans. Aerosp. Electron. Syst., AES-16, Jul 1980, pp. 509-516.
16. E.C. DuFort, "An Adaptive Low-Angle Tracking System," IEEE Trans. Antennas Propag., AP-29, Sep 1981, pp. 766-772.
17. N.L. Owsley, "Constrained Adaption," Array Processing Applications to Radar, Academic Press, 1980.
18. E. Brennan, J.D. Mallett, and I.S. Reed, "Adaptive Arrays in Airborne MTI Radar," IEEE Trans. Antennas and Propagation, AP-24, Sep 1976, pp. 607-615.
19. B.M. Leiner, "An Analysis and Comparison of Energy Direction Finding Systems," IEEE Trans. AES, AES-15, Nov 1979, pp. 861-873.
20. J.P. Shelton, "Focusing Characteristics of Symmetrically Configured Bootlace Lenses," IEEE Trans. Antennas and Propagation, AP-26, Jul 1978, pp. 513-518.
21. W.D. White, "Low-Angle Radar Tracking in the Presence of Multipath," IEEE Trans. AES, AES-10, Nov 1974, pp. 835-853.
22. R.C. Davis, L.E. Brennan and L.S. Reed, "Angle Estimation with Adaptive Arrays in External Noise Fields," IEEE Trans, AES, AES-12, Mar 1976, pp. 179-186.
23. W.D. White, "Angular Spectra in Radar Applications," IEEE Trans. Aerosp. Electron. Syst., AES-15, Nov 1979, pp. 895-899.
24. A. Cantoni and L. C. Godara, "Resolving the Directions of Sources in a Correlated Field Incident on an Array," Dept. of Electrical Engng., Univ. of Newcastle, Shortland, New South Wales, Australia, J. Acoustic. Soc. Am. (USA), 67, No. 4, Apr 1980, pp. 1247-1255.
25. B. Widrow, et al., "Signal Cancellation Phenomena in Adaptive Antennas: Causes and Cures," IEEE Trans. Antennas and Prop., AP-30, May 1982, pp. 469-478.
26. T.J. Shan and T. Kailath, "Adaptive Beamforming for Coherent Signals and Interference," IEEE Trans. Acoust., Speech, Signal Processing, ASSP-33, pp. 527-536 (1985).
27. W.F. Gabriel, "A High-Resolution Target-Tracking Concept Using Spectral Estimation Techniques," NRL Report 8797, May 1984.
28. A.H. Nuttall, "Spectral Analysis of a Univariate Process with Bad Data Points, via Maximum Entropy and Linear Predictive Techniques," NUSC-TR-5303, Naval Underwater Systems Center, New London, CT, Mar 1976.
29. L. Marple, "A New Autoregressive Spectrum Analysis Algorithm," IEEE Trans. Acoust., Speech, Signal Process. ASSP-28, Aug 1980, pp. 441-454.

Appendix A SNAPSHOT SIGNAL MODEL

Consider a simple linear array of K elements as shown in Fig. A1. The received signal samples are correlated in both space and time, giving rise to a two-dimensional data problem, but we convert this to spatial domain only by assuming that narrow-band filtering precedes our spatial domain processing. Bandwidth can be handled when necessary via a spectral line approach [A1] or tapped delay lines at each element [A2], but we did not consider such extra complication essential to the basic purposes of this analysis. Thus, the postulated signal environment on any given observation consists of I narrow-band plane waves arriving from distinct directions θ_i . The RF phase at the k th antenna element as a result of the i th source would be the product $\omega_i X_k$, where X_k is the location of the element phase center with respect to the midpoint of the array in wavelengths, and ω_i is defined as

$$\omega_i = 2\pi \sin \theta_i. \quad (\text{A1})$$

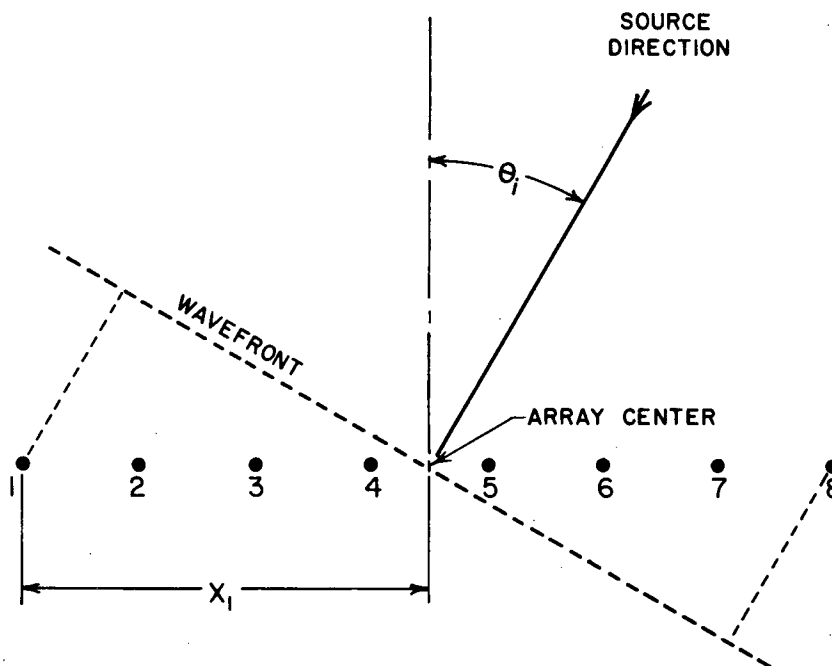


Fig. A1 — Geometry of linear array and signal wavefront

This notation is deliberately chosen to have the spatial domain dual of sampling in the time domain, so that the reader may readily relate to the more familiar spectral analysis variables. $\sin \theta_i$ is the dual of a sinusoid frequency f_i , and the X_k locations are the dual of time sampling instants t_k . Note that if our elements are equally spaced by a distance d , then X_k may be written,

$$X_k = \left(\frac{d}{\lambda} \right) \left(k - \left(\frac{K+1}{2} \right) \right) \quad (\text{A2})$$

where λ is the common RF wavelength. The ratio d/λ becomes the dual of the sampling time T with the cutoff frequency equal to half of the reciprocal.

The complex amplitude of the i th source at the array midpoint phase center is p_i , such that we can now express the n th time-sampled signal at the k th element as,

$$E_k(n) = \eta_k(n) + \sum_{i=1}^I p_i(n) g_k(\theta_i) \exp(j\omega_i X_k) \quad (\text{A3})$$

where $g_k(\theta_i)$ is the element pattern response in the direction θ_i , and $\eta_k(n)$ is the n th sample from the k th element independent Gaussian receiver noise. (The receiver noise component is assumed to be a random process with respect to both the time index n and the element index k .) Equation (A3) permits us to construct a convenient column vector of observed data in the form,

$$\mathbf{E}(n) = \mathbf{V}\mathbf{p}(n) + \boldsymbol{\eta}(n) \quad (\text{A4})$$

$$\begin{bmatrix} E_1(n) \\ E_2(n) \\ E_3(n) \\ \vdots \\ \vdots \\ \vdots \\ E_K(n) \end{bmatrix} = \begin{bmatrix} v_{11} & v_{21} & & v_{I1} \\ v_{12} & v_{22} & & v_{I2} \\ v_{13} & v_{23} & & v_{I3} \\ \vdots & \vdots & \dots & \vdots \\ \vdots & \vdots & \vdots & \vdots \\ \vdots & \vdots & \vdots & \vdots \\ v_{1K} & v_{2K} & & v_{IK} \end{bmatrix} \begin{bmatrix} p_1(n) \\ p_2(n) \\ \vdots \\ \vdots \\ p_I(n) \end{bmatrix} + \begin{bmatrix} \eta_1(n) \\ \eta_2(n) \\ \eta_3(n) \\ \vdots \\ \vdots \\ \vdots \\ \eta_K(n) \end{bmatrix}$$

where \mathbf{V} is a $K \times I$ matrix containing a column vector \mathbf{v}_i for each of the I source directions; i.e.,

$$v_{ik} = g_k(\theta_i) \exp(j\omega_i X_k). \quad (\text{A5})$$

Note that Eq. (A4) separates out the basic variables of source direction in the direction matrix \mathbf{V} , source baseband signal in the column vector $\mathbf{p}(n)$, and element receiver channel noise in the column vector $\boldsymbol{\eta}(n)$. The vector $\mathbf{E}(n)$ is defined as the n th snapshot, i.e., a simultaneous signal sampling across all K -array elements at the n th time instant. These snapshots would nominally occur at the Nyquist sampling rate corresponding to our receiver bandwidth [A3], so that a radar-oriented person may view them as range bin time samplings. However, for source estimation purposes, they need not necessarily be chosen from contiguous range bins, and for most applications it would be highly desirable to selectively time gate the snapshots used for source estimation. For this simple analysis, let us postulate that the snapshots are gated at more or less arbitrary instants of time.

Over typical processing intervals, the directions of arrival will not change significantly, so that \mathbf{V} is a slowly changing matrix. In contrast, the signals $p_i(n)$ will generally vary rapidly with time, often unpredictably, such that we must work with their statistical descriptions. It is assumed that the signals are uncorrelated with receiver noise. Proceeding then from Eq. (A4), we can obtain the covariance matrix \mathbf{R} via application of the expected value operator, \mathcal{E} , or ensemble average,

$$\mathbf{R} = \mathcal{E}[\mathbf{E}(n)\mathbf{E}^*(n)] \quad (\text{A6})$$

$$\mathbf{R} = \mathbf{V}\mathbf{P}\mathbf{V}^t + \mathbf{N} \quad (\text{A7})$$

where $\mathbf{N} = \mathcal{E}[\boldsymbol{\eta}(n)\boldsymbol{\eta}(n)^*]$, $\mathbf{P} = \mathcal{E}[\mathbf{p}(n)\mathbf{p}(n)^*]$, $*$ is the complex conjugate, and t is the transpose. \mathbf{N} is a simple diagonal matrix consisting of the receiver channel noise power levels. The diagonal elements of \mathbf{P} represent the ensemble average power levels of the various signal sources, and off-diagonal elements can be nonzero if any correlation exists between the sources. Note that correlated far-field signals can easily arise if significant specular reflection or diffraction multipath is present.

REFERENCES

- A1. W.F. Gabriel, "Adaptive Arrays — An Introduction," Proc. IEEE, **64**, Feb 1976, pp. 239-272.
- A2. E. Brennan, J.D. Mallett, and I.S. Reed, "Adaptive Arrays in Airborne MTI Radar," IEEE Trans. Antennas and Propagation, **AP-24**, Sep 1976, pp. 607-615.
- A3. O.V. Oppenheim and R.W. Schaffer, *Digital Signal Processing* (Prentice Hall, Englewood Cliffs, NJ, 1975).

Appendix B

EIGENVALUE/EIGENVECTOR DECOMPOSITION

When a signal is known to consist of pure sinusoids in white noise, an appropriate procedure to find the unknown frequencies and powers is the Pisarenko spectral-decomposition procedure [B1]. Although Pisarenko's method per se has not found widespread use, it has provided a fundamental eigenanalysis basis for several closely related techniques which have demonstrated excellent performance. Among these are the algorithms described by Reddi [B2], the MUSIC algorithm of Schmidt [B3], the work of Bienvenu and Kopp [B4], the singular value decomposition (or principal eigenvector) methods of Kumaresan and Tufts [B5,B6], the eigenassisted method of Evans et al. [B7], and the algebraic approach of Bronez and Cadzow [B8].

A key principle in all of these techniques is the geometric vector space relationships between the spatial source vectors and the eigenvectors of the sample covariance matrix; so we begin our discussion on this point. From the theory of matrices, we know that a positive definite Hermitian matrix such as \mathbf{R} of Eq. (A7), can be diagonalized by a nonsingular orthonormal modal matrix transformation which shall be defined as the matrix \mathbf{Q} . Furthermore, we know that the resulting diagonal components are the eigenvalues of matrix \mathbf{R} . In accordance with the usual eigenvalue problem statements,

$$|\mathbf{R} - \beta_i^2 \mathbf{I}| = 0 \text{ and } \mathbf{R}\mathbf{e}_i = \beta_i^2 \mathbf{e}_i, \quad (\text{B1})$$

the β_i^2 are the eigenvalues (real positive numbers) of \mathbf{R} , \mathbf{I} is the identity matrix, and \mathbf{e}_i are the associated eigenvectors. These eigenvectors, which are normalized to unit Hermitian length and are orthogonal to one another, make up the columns of the \mathbf{Q} matrix,

$$\mathbf{Q} = \begin{bmatrix} | & | & | & \cdots & | \\ \mathbf{e}_1 & \mathbf{e}_2 & \mathbf{e}_3 & \cdots & \mathbf{e}_K \\ | & | & | & & | \end{bmatrix} \text{ where } \mathbf{e}_i = \begin{bmatrix} e_{i1} \\ e_{i2} \\ e_{i3} \\ \vdots \\ e_{iK} \end{bmatrix} \quad (\text{B2})$$

Diagonalization of \mathbf{R} by the \mathbf{Q} matrix transformation per Eq. (B1) may be written,

$$[\mathbf{Q}^t \mathbf{R} \mathbf{Q}] = [\beta_i^2 \delta_{ij}] = \begin{bmatrix} \beta_1^2 & 0 & 0 & \dots & \dots \\ 0 & \beta_2^2 & 0 & \dots & \dots \\ 0 & 0 & \beta_3^2 & \dots & \dots \\ \dots & \dots & \dots & \dots & \dots \\ \dots & \dots & \dots & \dots & \dots \\ \dots & \dots & \dots & \dots & \beta_k^2 \end{bmatrix} \quad (\text{B3})$$

where δ_{ij} is the Kronecker delta symbol. One can readily show a construction of \mathbf{R} from its orthonormal components,

$$\mathbf{R} = \mathbf{Q}[\beta_i^2 \delta_{ij}] \mathbf{Q}^t = \sum_{k=1}^K \beta_k^2 \mathbf{e}_k \mathbf{e}_k^t \quad (\text{B4})$$

Next, we introduce the term "principal eigenvector" (PE) to mean those eigenvectors which correspond to the unique eigenvalues generated by the spatial source distribution; and the term "noise eigenvector" to mean those eigenvectors which correspond to the small noise eigenvalues generated by the receiver channel noise in Eq. (A7). Under ideal conditions, the noise eigenvalues are all identical and equal to receiver channel noise power level β_δ^2 , such that we can factor Eq. (B4) to emphasize the PE,

$$\mathbf{R} = \sum_{i=1}^q (\beta_i^2 - \beta_\delta^2) \mathbf{e}_i \mathbf{e}_i^t + \beta_\delta^2 \mathbf{I} \quad (\text{B5})$$

where q is the number of PE. Comparing Eq. (B5) with Eq. (A7) we note that the noise diagonal matrices are equal; i.e.,

$$\beta_\delta^2 \mathbf{I} = \mathbf{N} \quad (\text{B6})$$

so that one may equate the source direction vectors with the PE,

$$\mathbf{V} \mathbf{P} \mathbf{V}^t = \sum_{i=1}^I |\bar{p}_i|^2 \mathbf{v}_i \mathbf{v}_i^t = \sum_{i=1}^q (\beta_i^2 - \beta_\delta^2) \mathbf{e}_i \mathbf{e}_i^t \quad (\text{B7})$$

where the $|\bar{p}_i|^2$ represents the expected power levels of uncorrelated sources. Equation (B7) embodies the key principle that the PE are linear combinations of the source direction vectors and vice-versa. In geometrical language, the \mathbf{v}_i define an I dimensional source vector space, and the principal \mathbf{e}_i span that same vector space. Furthermore, since the noise eigenvectors are always orthogonal to the PE, then it follows that the noise eigenvectors must occupy a subspace which is orthogonal to the source vector space. To put it another way, if the noise eigenvectors are viewed as antenna array element weights, then they should have pattern nulls at source direction angles because of their orthogonality. (Note the vivid demonstration of this point in Fig. 3(b).) Despite the fact that Eq. (B7) is based on ideal assumptions, it turns out to be a valuable concept for formulating algorithms, perhaps because it is inherently a noise-subtracted relationship, and the estimates of the PE are rather robust.

When working with finite sets of data snapshots which are not ideal, a nontrivial problem area arises in determining which eigenvectors to designate as principal, and which ones result from noise. This important problem will be addressed after discussing the associated algorithms.

Eigenanalysis of Three Algorithms

Eigenvalue/eigenvector decomposition is now applied to three different spatial spectrum estimation algorithms:

- the MLM (Maximum Likelihood Method),
- the MUSIC (Multiple Signal Classification), and
- the PEGS (Principal Eigenvector Gram-Schmidt).

Since these algorithms are dealt with in a very abbreviated manner in the report, the reader is encouraged to consult the references given for a better description and understanding of the techniques involved.

The MLM (Maximum Likelihood Method)

The maximum likelihood spectral estimate is defined as a filter designed to pass the power in a narrow-band about the signal frequency of interest and to minimize or reject all other frequency components in an optimal manner [B9,B10]. This is identical to the use of a zero-order mainbeam directional gain constraint in adaptive arrays [B11], where the spatial spectrum would be estimated by the output residual power P_0 from the optimized adapted array weights,

$$P_0(\theta) = \mathbf{W}_0^* \mathbf{R} \mathbf{W}_0. \quad (\text{B8})$$

Where \mathbf{W}_0 is the optimum adaptive Wiener filter weight, and

$$\mathbf{W}_0 = \mu \mathbf{R}^{-1} \mathbf{S}^* \quad (\text{B9})$$

where \mathbf{S}^* is the usual mainbeam weight vector for steering angle θ , and μ is a complex number. Under the zero-order gain constraint, we require $\mathbf{S}' \mathbf{W}_0 = 1$, whereupon μ becomes

$$\mu = [\mathbf{S}' \mathbf{R}^{-1} \mathbf{S}^*]^{-1}. \quad (\text{B10})$$

Substituting μ and \mathbf{W}_0 into Eq. (B8) results in

$$P_0(\theta) = \left[\frac{1}{\mathbf{S}' \mathbf{R}^{-1} \mathbf{S}^*} \right]. \quad (\text{B11})$$

Upon sweeping the steering vector \mathbf{S}^* for a given covariance matrix inverse, $P_0(\theta)$ estimates the spatial spectrum.

In terms of eigenvalue/eigenvector decomposition, we can take the inverse of Eq. (B3) and express \mathbf{R}^{-1} in the form,

$$\mathbf{R}^{-1} = \mathbf{Q} \begin{bmatrix} \delta_{ij} \\ \beta_i^2 \end{bmatrix} \mathbf{Q}^* = \sum_{k=1}^K \left(\frac{1}{\beta_k^2} \right) \mathbf{e}_k \mathbf{e}_k^*. \quad (\text{B12})$$

Here, we see that this older algorithm simply uses all of the eigenvalues/eigenvectors. One advantage in this decomposition is that Eq. (B12) can be substituted into Eq. (B11) to form a simple summation of eigenvector beams referenced to the receiver noise power level,

$$\left(\frac{P_0(\theta)}{\beta_0^2} \right) = \frac{1}{\sum_{k=1}^K \left(\frac{\beta_0^2}{\beta_k^2} \right) g_k^2(\theta)} \quad (\text{B13})$$

where $g_k(\theta) = \mathbf{S}'\mathbf{e}^k$. This permits an insight into the peak values which occur at the nulls of the noise eigenvector beams; i.e., we get an evaluation of relative source power level if the source location is resolved.

The MUSIC (Multiple Signal Classification)

This algorithm was suggested by Schmidt [B3] to provide asymptotically unbiased estimates of the number of signal sources, directions of arrival, strengths and cross correlations among the directional waveforms, polarizations, and strength of noise/interference. His geometrical vector space description and interpretation is clearly presented and was used as the basis for the one above. Essentially, this MUSIC algorithm selects and uses only the noise eigenvectors to solve for the directions of arrival. This is tantamount to approximating \mathbf{R}^{-1} in Eq. (B11) by the noise eigenvectors only; i.e.,

$$\text{let } \mathbf{R}^{-1} \approx \sum_{i=q+1}^K \left(\frac{1}{\beta_i^2} \right) \mathbf{e}_i \mathbf{e}_i^* \quad (\text{B14})$$

where q is the number of principal eigenvectors. The same indexing would apply as noise eigenvector beams in Eq. (B13), where we note that the ratio of eigenvalues would now become unity (or close to it).

This algorithm does indeed produce very large peaks in $P_0(\theta)$ for good covariance matrix estimates, because of the aforementioned orthogonality of the noise eigenvectors to the source vector space. Its performance is usually far superior to the older MLM algorithm in resolving closely spaced source directions. In addition, Schmidt points out that once the directions of arrival have been found, the direction matrix \mathbf{V} , in Eq. (A4) and (A7) becomes available and may be used to compute the source power matrix \mathbf{P} . We form the special matrix \mathbf{U} ,

$$\mathbf{U} = [\mathbf{V}^* \mathbf{V}]^{-1} \mathbf{V}^* \quad (\text{B15})$$

and

$$\mathbf{U} \mathbf{V} \mathbf{P} \mathbf{V}^* \mathbf{U}^* = \mathbf{P}.$$

If the matrix \mathbf{U} exists or can be closely approximated, then we can apply it to the noise-subtracted covariance matrix of Eq. (A7) to solve for \mathbf{P} ; i.e.,

$$\mathbf{P} = \mathbf{U}(\mathbf{R} - \mathbf{N})\mathbf{U}^* \quad (\text{B16})$$

$$\mathbf{P} = \begin{bmatrix} \overline{p_1^* p_1} & \overline{p_1^* p_2} & \cdots & \overline{p_1^* p_l} \\ \overline{p_2^* p_1} & \overline{p_2^* p_2} & \cdots & \overline{p_2^* p_l} \\ \cdot & \cdot & \cdot & \cdot \\ \cdot & \cdot & \cdot & \cdot \\ \cdot & \cdot & \cdot & \cdot \\ \overline{p_l^* p_1} & \overline{p_l^* p_2} & \cdots & \overline{p_l^* p_l} \end{bmatrix}$$

Note that the diagonal elements of \mathbf{P} represent power estimates of the sources, and that the nonzero off-diagonal elements represent estimates of the correlations existing between partially coherent sources.

The ability to solve for the power estimates is of great importance in distinguishing "false alarms" and in selecting the sources of interest. We recommend References B7, B6, and B8 which are either related to or give a comparative analysis of the MUSIC algorithm.

The PEGS (Principal Eigenvector Gram-Schmidt)

Several eigenvalue/eigenvector decomposition techniques described in References B7, B2, B6, and B8 are based on the principal eigenvectors (PE) with some type of constraint imposed on the optimum weight vector.

This subgroup of PE methods is of interest in the current work because of their generally superior performance characteristics. An intuitive reasoning behind their use is that the estimates of the PE are robust; i.e., they tend to remain relatively stable from one data record to the next, whereas the noise eigenvectors tend to fluctuate because of noise perturbations. In addition, the PE methods are inherently a noise subtraction technique similar to noise power cancellation algorithms which attempt to remove the noise bias term that appears along the main diagonal of the covariance matrix.

Let us begin development of our PEGS algorithm by decomposing the inverse of the covariance matrix as given in Eq. (B12), normalized by receiver noise power,

$$\begin{aligned}\beta_0^2 \mathbf{R}^{-1} &= \sum_{k=1}^K \left(1 - \frac{\beta_k^2 - \beta_0^2}{\beta_k^2} \right) \mathbf{e}_k \mathbf{e}_k^* \\ &= \mathbf{I} - \sum_{i=1}^q \left(\frac{\beta_i^2 - \beta_0^2}{\beta_i^2} \right) \mathbf{e}_i \mathbf{e}_i^*\end{aligned}\quad (\text{B17})$$

Substituting Eq. (B17) into Eq. (B9) results in the optimum Wiener weight,

$$\begin{aligned}\mathbf{W}_0 &= \frac{\mu}{\beta_0^2} \left[\mathbf{I} - \sum_{i=1}^q \left(\frac{\beta_i^2 - \beta_0^2}{\beta_i^2} \right) \mathbf{e}_i \mathbf{e}_i^* \right] \mathbf{S}^* \\ &= \mu' \left[\mathbf{S}^* - \sum_{i=1}^q \left(\frac{\beta_i^2 - \beta_0^2}{\beta_i^2} \right) \alpha_i \mathbf{e}_i \right]\end{aligned}\quad (\text{B18})$$

where:

$$\alpha_i = \mathbf{e}_i^* \mathbf{S}^*,$$

$$\mu' = \mu / \beta_0^2, \text{ and}$$

\mathbf{S}^* = a quiescent array weight vector.

In the limit of noise-free data, Eq. (B18) is suggestive of a simple Gram-Schmidt vector subtraction from \mathbf{S}^* in which we would form an optimum weight that would be orthogonal to the PE, and therefore, orthogonal to the source direction vectors per Eq. (B7). Thus, let us formulate a PEGS algorithm by defining the optimum weight \mathbf{W}_e from Eq. (B18) as

$$\mathbf{W}_e = \mathbf{S}^* - \sum_{i=1}^q \alpha_i \mathbf{e}_i \quad (\text{B19})$$

where:

$$\alpha_i = \mathbf{e}_i^* \mathbf{S}^*.$$

\mathbf{W}_e possesses the necessary orthogonality to noise-free source direction vectors,

$$\langle \mathbf{W}_e, \mathbf{v}_i \rangle = 0 \quad (\text{B20})$$

and may readily incorporate the option of unit Hermitian length if desired,

$$|W_e|^2 = 1. \quad (\text{B21})$$

The PEGS algorithm as applied in this report used an end-element weighting for S^* ; i.e.,

$$S^* = [0 \ 0, \dots, 0, 1]^t. \quad (\text{B22})$$

Culling Principal Eigenvalues

The number of principal eigenvalues is usually directly related to the number of sources which, in practice, are not known and must be estimated. One of the early estimation techniques which has often been used is the AIC (Akaike Information Criterion) [B12,B13]. This criterion has been successfully applied to many model identification problems in engineering and statistics, including the well known problem of determining the order of an autoregressive (AR) process [B13]. Recent work reported by Wax and Kailath [B14] presents a new approach based on the AIC, which eliminates the need for any subjective judgment in the decision process; i.e., the procedure does not require any subjectively chosen threshold. This new approach was implemented during the current investigation and was found to be very effective for most of the examples tested. In addition to the Wax-Kailath AIC approach, we also used a second effective technique which is based on the following three processing operations:

- An initial decreasing-magnitude sort,
- Culling per coarse magnitude threshold, and
- Culling per sensitive threshold based on a quadratic curvefit predictor.

The entire procedure is listed in Ref. [B15] as a Fortran IV computer code.

REFERENCES

- B1. V.F. Pisarenko, "The Retrieval of Harmonics from a Covariance Function," *Geophys. J. (Royal Astron. Soc.)* **33**, 1973, pp. 347-366.
- B2. S.S. Reddi, "Multiple Source Location — A Digital Approach," *IEEE Trans. Aerospace & Elect. Sys.*, AES-15, Jan 1979, pp. 95-105.
- B3. R. Schmidt, "Multiple Emitter Location and Signal Parameter Estimation," *Proc. of the RADC Spectrum Estimation Workshop, RADC-TR-79-63*, Rome Air Development Center, Rome, NY, Oct 1979, p. 243.
- B4. E. Bienvenu and L. Kopp, *Adaptive High Resolution Spatial Discrimination of Passive Sources, Underwater Acoustics and Signal Processing* (D. Reidel Publishing Co., Boston, 1981), pp. 509-515.
- B5. R. Kumaresan and D. Tufts, "Singular Value Decomposition and Spectral Analysis," *Proc. of the First ASSP Workshop on Spectral Estimation, McMaster University, Hamilton, Ontario, Canada*, 2, Aug 1981, pp. 6.4.1-6.4.12.
- B6. R. Kumaresan and D.W. Tufts, "Estimating the Angles of Arrival of Multiple Plane Waves," *IEEE Trans. Aerospace & Elect. Sys.*, AES-19, Jan 1983, pp. 134-139.
- B7. J.E. Evans, J.R. Johnson, and D.F. Sun, "Application of Advanced Signal Processing Techniques to Angle of Arrival Estimation in ATC Navigation and Surveillance Systems," *MIT Lincoln Laboratory Tech. Report 582, (FAA-RD-82-42)*, Jun 1982.

- B8. T.P. Bronez and J.A. Cadzow, "An Algebraic Approach to Superresolution Array Processing," IEEE Trans. Aerospace & Elect. Sys., AES-19, Jan 1983, pp. 123-133.
- B9. D.G. Childers, ed., Modern Spectrum Analysis, IEEE Press, New York, N.Y. 1978.
- B10. W.F. Gabriel, "Spectral Analysis and Adaptive Array Superresolution Techniques," Proc. IEEE 68, Jun 1980, pp. 654-666.
- B11. S.P. Applebaum and D.J. Chapman, "Adaptive Array with Main Beam Constraints," IEEE Trans. Antenna Propagat. AP-24, Sep 1976, pp. 650-662.
- B12. H. Akaike, *Statistical Predictor Identification*, (Ann. Inst. Statis. Math. 22, p. 205, 1970).
- B13. H. Akaike, "A New Look at the Statistical Model Identification," IEEE Trans. Autom. Contr. AC-19, 1974, pp. 716-723.
- B14. M. Wax and T. Kaliath, "Determining the Number of Signals by Information Theoretic Criteria," Proc. of the IEEE/ASSP Spectrum Estimation Workshop II, Tampa, FL, Nov 1983 pp. 192-193.
- B15. W.F. Gabriel, "A High-Resolution Target-Tracking Concept Using Spectral Estimation Techniques," NRL Report 8797, May 1984.

Appendix C

TRACKING BEAMS AND ADAPTIVE DISTORTION

The tracking beams used in Section, An Adaptive Array Tracking Application, are based on the selection of an adjacent pair of orthogonal uniform illumination beams generated by a Butler matrix beamformer [C1] transformation. The transformation matrix \mathbf{B} for a linear array with half-wavelength element spacing will have individual matrix components of the form,

$$b_{km} = \frac{1}{\sqrt{K}} \exp \left\{ \frac{2\pi}{K} \left(k - \frac{K+1}{2} \right) \left(m - \frac{K+1}{2} \right) \right\} \quad (\text{C1})$$

where:

m = beam index

k = element index

K = total number of elements.

$$\mathbf{B} = \begin{bmatrix} b_{11} & b_{12} & \dots & b_{1K} \\ b_{21} & b_{22} & \dots & b_{2K} \\ b_{31} & b_{32} & \dots & b_{3K} \\ \cdot & \cdot & \dots & \cdot \\ \cdot & \cdot & \dots & \cdot \\ \cdot & \cdot & \dots & \cdot \\ b_{K1} & b_{K2} & \dots & b_{KK} \end{bmatrix} \quad (\text{C2})$$

The beamformer output vector $\hat{\mathbf{E}}$ is expressed,

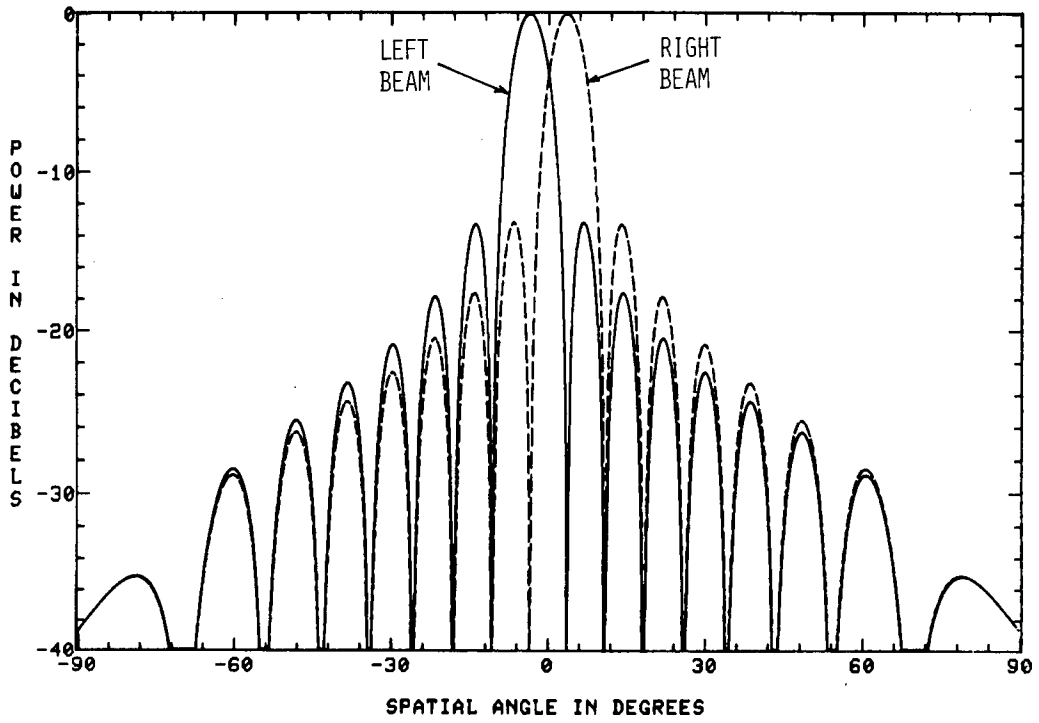
$$\hat{\mathbf{E}} = \mathbf{B}'\mathbf{E} \quad (\text{C3})$$

Figure C1(a) illustrates typical $\text{sinc}x/x$ patterns of an adjacent pair of beams for our 16-element array example. The familiar sum (Σ) and difference (Δ) tracking beam outputs are then obtained from this adjacent pair via the 3 dB hybrid junction as shown in Fig. C2, where we note that the Δ beam is in quadrature phase relationship to the Σ beam. Expressed in terms of element weights, the Σ beam weight vector \mathbf{S} and the Δ beam weight vector \mathbf{D} may be written via Eq. (C2),

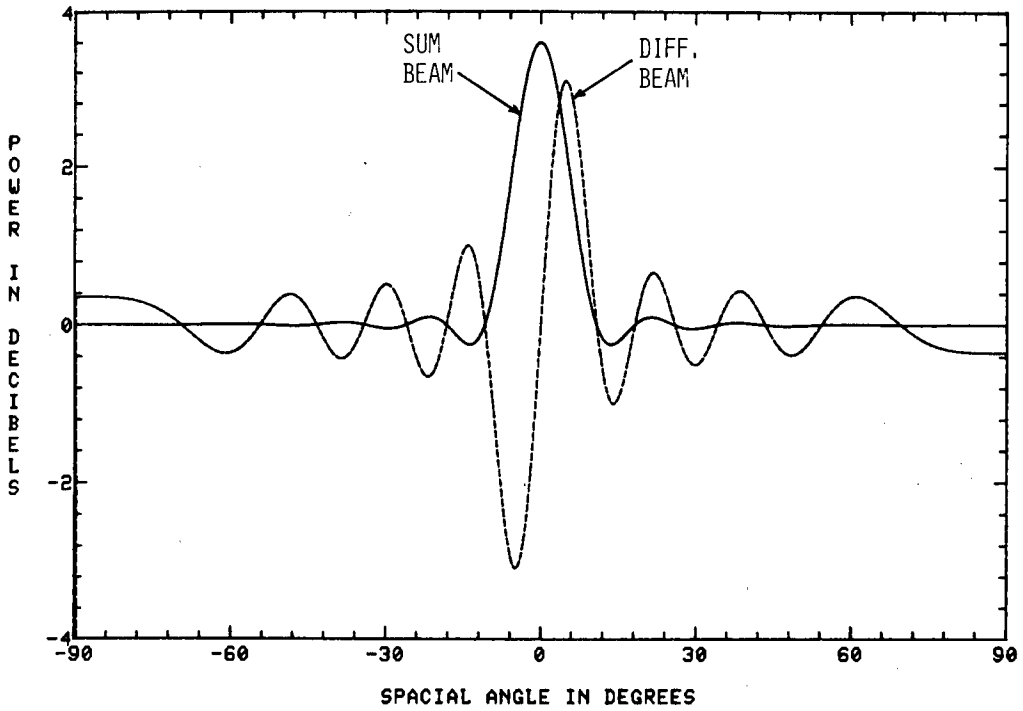
$$\begin{aligned} \mathbf{S} &= \frac{1}{2} [\mathbf{b}_{m+1} + \mathbf{b}_m] \\ \mathbf{D} &= \frac{1}{2} [\mathbf{b}_{m+1} - \mathbf{b}_m]. \end{aligned} \quad (\text{C4})$$

The uniform illumination vectors \mathbf{b}_m and \mathbf{b}_{m+1} result in cosine illuminations for \mathbf{S} and \mathbf{D} , which are shown plotted in Fig. C1(b) for our 16-element linear array example.

Monopulse tracking [C2] involves an angle estimate for each pulse (snapshot) containing the target, and it is computed from the ratio of Δ/Σ . From the cosine illumination beams of Fig. C1, note that we can form the approximation,



(a) Adjacent pair of Butler matrix beams



(b) Resultant sum and difference beams

Fig. C1 — Tracking beams formed for 16 element linear array

$$\left(\frac{\Delta}{\Sigma}\right) \approx C \left(\frac{\sin\psi}{1 + \cos\psi}\right) = C \tan\left(\frac{\psi}{2}\right) \quad (C5)$$

where

$$\psi = \left(\frac{\pi}{2}\right) \left(\frac{\delta}{B}\right),$$

δ is the angle of the target from boresight,

B is the angle to the first null of the sum pattern, and

C is a constant which depends upon the particular illuminations.

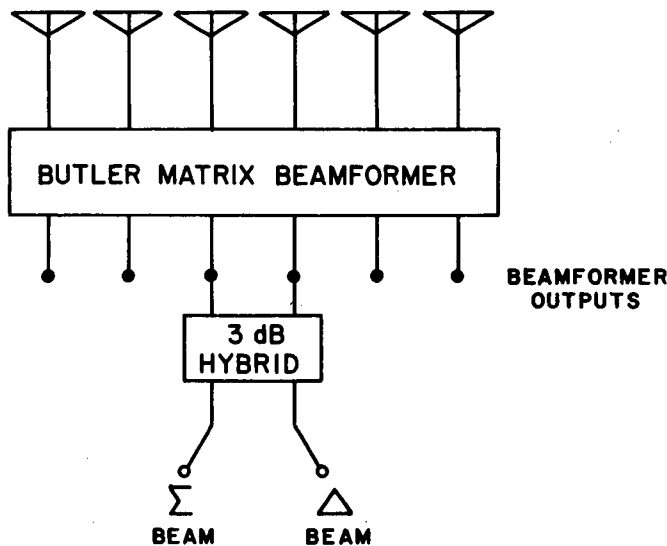


Fig. C2 — Block diagram of tracking beam formation via Butler matrix beamformer

For our example, $C = 3.8^\circ$ and $B = 10.8^\circ$. Thus, given values of Δ/Σ , we can solve for track angle estimates, δ/B , from Eq. (C5).

Next, let us address track estimate distortion. Whenever one performs spatial filtering as described in Section, All-Digital Tracking System Concept, a distortion of received plane wavefronts occurs because the spatial insertion loss generally varies as a function of $\sin \theta$.

This problem was first addressed in the literature by Davis, Brennan, and Reed [C3] who proposed an algorithm for estimating the angle of arrival, based on the outputs of adaptively distorted sum and difference beams. They used approximations to the optimum angle estimator which permitted correction of distortion at the tracking beam boresight position, and they demonstrated good performance via simulation for sidelobe and/or mainbeam interference.

In an all-digital system, we know our adaptive filter weights. Therefore, we can compute the resultant distortion error throughout the tracking beam region. In Section, All-Digital Tracking System Concept, above, we showed that it makes no difference whether we apply our quiescent beam weights to the spatially filtered signals, or the equivalent adaptive weights to the unfiltered signals. Thus, we

may apply the monopulse sum and difference weights of Eq. (C4) to the spatially filtered output residue signal vector of Eqs. (11, 12) in Section, All-Digital Tracking System Concept, and obtain the equivalent forms,

$$\Sigma = \mathbf{S}'\mathbf{E}_f = \mathbf{E}'\mathbf{M}^{-1}\mathbf{S} = \mathbf{E}'\mathbf{W}_s \quad (\text{C6})$$

and

$$\Delta = \mathbf{D}'\mathbf{E}_f = \mathbf{E}'\mathbf{M}^{-1}\mathbf{D} = \mathbf{E}'\mathbf{W}_d, \quad (\text{C7})$$

where \mathbf{W}_s and \mathbf{W}_d are now the equivalent adapted (and distorted) sum and difference beam weights. The distorted ratio Δ/Σ can be computed for any direction vector \mathbf{E} , thus giving us the distortion curve across the entire tracking angle region.

REFERENCES

- C1. J. Butler, "Multiple Beam Antennas," Sanders Assoc. Internal Memo RF 3849, Jan 1960.
- C2. Merrill Skolnik, *Radar Handbook* (McGraw-Hill Book Co., NY, 1970).
- C3. R.C. Davis, L.E. Brennan and L.S. Reed, "Angle Estimation with Adaptive Arrays in External Noise Fields," IEEE Trans, AES, AES-12, Mar 1976, pp. 179-186.

Appendix D

FORWARD-BACKWARD SUBAPERTURE AVERAGING

This is an excellent technique for increasing the effective averaging of our sample covariance matrix SCM when needed, and it may readily be implemented if the antenna array elements are identical and equally spaced. Figure D1 illustrates this technique. We form a reduced dimension subaperture of L elements, where L must be less than the total number of array elements K . Starting from the left-hand side, the subaperture samples its first snapshot as elements 1 through L , then bumps to the right by 1 and samples its second snapshot as elements 2 through $(L + 1)$, then bumps to the right by 1 and samples its third snapshot as elements 3 through $(L + 2)$, etc. After bumping across to the K th element, we will have accumulated $(K - L + 1)$ subaperture snapshots from one overall array data snapshot, such that we can increase our SCM averaging by that same factor. This subaperture motion from left to right produces what is generally termed "forward averaging." The technique may be applied to any SCM method. For example, the simple block averaging of Eq. (2) in section, Low-Sidelobe Eigenvector Constraint becomes

$$\hat{\mathbf{R}}_f = \frac{1}{N(K - L + 1)} \sum_{n=1}^N \sum_{i=1}^{(K-L+1)} [\mathbf{E}(n, i) \mathbf{E}(n, i)^*] \quad (\text{D1})$$

where $\mathbf{E}(n, i)^t = [E_i(n), E_{i+1}(n), \dots, E_{i+L-1}(n)]$ and $\hat{\mathbf{R}}_f$ is the new reduced $L \times L$ dimension SCM. Note that $\mathbf{E}(n, i)$ may be expressed as the matrix product,

$$\mathbf{E}(n, i) = \mathbf{I}_i \mathbf{E}(n) \quad (\text{D2})$$

where \mathbf{I}_i is a special $L \times K$ rectangular sampling matrix in which the i index denotes the first column where the identity matrix \mathbf{I} begins. For example, the \mathbf{I}_i matrix for $L = 3$, $K = 6$, and $i = 2$ would be

$$\mathbf{I}_i = [\mathbf{O} \mid \mathbf{I}_L \mid \mathbf{O}] \quad (\text{D3})$$

$$\mathbf{I}_2 = \begin{bmatrix} 0 & 1 & 0 & 0 & 0 & 0 \\ 0 & 0 & 1 & 0 & 0 & 0 \\ 0 & 0 & 0 & 1 & 0 & 0 \end{bmatrix}$$

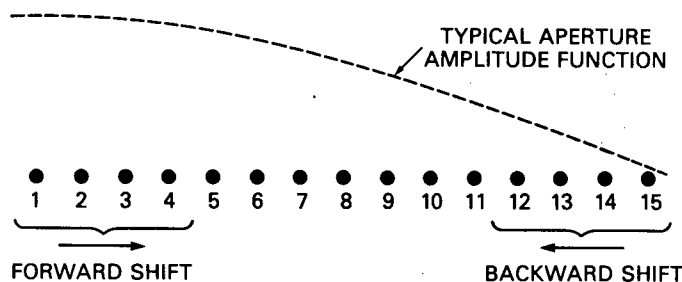


Fig. D1 - Forward-backward shift movement for a reduced dimension sampling subaperture where $L = 4$, along a linear antenna array of $K = 15$ elements

An \mathbf{I}_i matrix may be used to reduce the number of computations by multiplying the SCM to obtain

$$\hat{\mathbf{R}}_f = \frac{1}{(K - L + 1)} \sum_{i=1}^{(K-L+1)} [\mathbf{I}_i \hat{\mathbf{R}} \mathbf{I}_i^t] \quad (\text{D4})$$

Equations (D4) and (D1) give similar results, and both are mathematical expressions of the additional spatial averaging or "smoothing" that is obtained via the moving subaperture technique.

Furthermore, the averaging can be doubled again by reversing our subaperture at the right-hand side and bumping across to the left-hand side in similar fashion; however, it requires conjugating the subaperture snapshots. This subaperture motion from right to left produces what is generally termed "backward-averaging."

If we define the reversed and conjugated vector, E^{\dagger} , in terms of our array element data samples of equation (A3), then the k th element signal sample becomes

$$E_k^{\dagger} = E_{K-k+1}^* ; \quad k = 1, 2, 3, \dots, K \quad (D5)$$

The reader can verify that the resulting SCM will be an index-exchanged \hat{R}_f^{\dagger} , and that we can combine the two into a final forward-backward average SCM which is denoted as the reduced $L \times L$ matrix \hat{R}_{fb} :

$$\hat{R}_{fb} = 1/2 [\hat{R}_f + \hat{R}_f^{\dagger}]. \quad (D6)$$

Note that \hat{R}_{fb} is a symmetric matrix, but is generally not Toeplitz. References D1 and D2 are recommended for further detailed discussion of the technique.

Although forward-backward subaperture averaging is a very simple concept, it usually produces remarkable improvements in output estimates, and it becomes crucial to processing in the following situations:

- When only a few data snapshots are available per SCM computation. Note that the method can be used even under the extreme condition of only a single snapshot.
- When significant coherence exists between spatial sources as for example in multipath situations involving a specular reflection. For this particular condition, the fields arriving at the aperture are nonstationary in space and the SCM is not Toeplitz [D1,D3,D4,D5].

A caveat concerning this averaging technique is that, as the dimension L of the subaperture becomes smaller, the subaperture antenna gain, resolution, and degrees of freedom decrease. Thus, the advantage of increased averaging must always be balanced against these factors, and it is usually prudent to process with as large a subaperture dimension as possible.

REFERENCES

- D1. J.E. Evans, J.R. Johnson, and D.F. Sun, "Application of Advanced Signal Processing Techniques to Angle of Arrival Estimation in ATC Navigation and Surveillance Systems," MIT Lincoln Laboratory Tech. Report 582, (FAA-RD-82-42), Jun 1982.
- D2. A.H. Nuttall, "Spectral Analysis of a Univariate Process with Bad Data Points, via Maximum Entropy and Linear Predictive Techniques," NUSC-TR-5303, Naval Underwater Systems Center, New London, CT, Mar 1976.
- D3. T.J. Shan and T. Kailath, "Adaptive Beamforming for Coherent Signals and Interference," IEEE Trans. Acoust., Speech, Signal Processing, Vol. ASSP-33, pp. 527-536, (1985).
- D4. W.D. White, "Angular Spectra in Radar Applications," IEEE Trans. Aerosp. and Electron. Syst., AES-15, Nov 1979, pp. 895-899.
- D5. W.F. Gabriel, "Spectral Analysis and Adaptive Array Superresolution Techniques," Proc. IEEE 68, Jun 1980, pp. 654-666.